

# NAVAL POSTGRADUATE SCHOOL

## Monterey, California



## THESIS

**PROPAGATION OF A TWO-PHASE DETONATION  
ACROSS A GEOMETRIC DIFFRACTION WITH  
COMPOSITIONAL DISCONTINUITY**

by

Todd A. Hofstedt

June 2000

Thesis Advisor:

Co-Advisor:

Second Reader:

Christopher M. Brophy

David W. Netzer

Raymond P. Shreeve

Approved for public release; distribution is unlimited.

DTIC QUALITY INSPECTED 4

20000825 029

<b>REPORT DOCUMENTATION PAGE</b>			Form Approved OMB No. 0704-0188	
Public reporting burden for this collection of information is estimated to average 1 hour per response, including the time for reviewing instruction, searching existing data sources, gathering and maintaining the data needed, and completing and reviewing the collection of information. Send comments regarding this burden estimate or any other aspect of this collection of information, including suggestions for reducing this burden, to Washington headquarters Services, Directorate for Information Operations and Reports, 1215 Jefferson Davis Highway, Suite 1204, Arlington, VA 22202-4302, and to the Office of Management and Budget, Paperwork Reduction Project (0704-0188) Washington DC 20503.				
<b>1. AGENCY USE ONLY (Leave blank)</b>		<b>2. REPORT DATE</b> June 2000	<b>3. REPORT TYPE AND DATES COVERED</b> Engineer's Thesis	
<b>4. TITLE AND SUBTITLE :</b> Propagation of a Two-Phase Detonation Across a Geometric Diffraction with Compositional Discontinuity			<b>5. FUNDING NUMBERS</b> N0001400WR20216	
<b>6. AUTHOR(S)</b> Hofstedt, Todd A.				
<b>7. PERFORMING ORGANIZATION NAME(S) AND ADDRESS(ES)</b> Naval Postgraduate School Monterey, CA 93943-5000			<b>8. PERFORMING ORGANIZATION REPORT NUMBER</b>	
<b>9. SPONSORING / MONITORING AGENCY NAME(S) AND ADDRESS(ES)</b> Office of Naval Research Ballston Tower One 800 N. Quincy Street Arlinton, VA 22217-5660			<b>10. SPONSORING / MONITORING AGENCY REPORT NUMBER</b>	
<b>11. SUPPLEMENTARY NOTES</b> The views expressed in this thesis are those of the author and do not reflect the official policy or position of the Department of Defense or the U.S. Government.				
<b>12a. DISTRIBUTION / AVAILABILITY STATEMENT</b> Approved for public release; distribution is unlimited.			<b>12b. DISTRIBUTION CODE</b>	
<b>13. ABSTRACT (maximum 200 words)</b>  The research program involved the modification and use of an existing pulse detonation engine (PDE) to investigate the detonability of a JP-10/air aerosol. The detonation of a JP-10 aerosol in air proved more difficult than was originally anticipated. The use of a small JP-10/oxygen pre-detonator to provide direct initiation results in a transition region with a geometric diffraction and compositional discontinuity. Propagation of a detonation into such a region is very complex but critical to the re-establishment of the detonation wave in the JP-10/air mixture. A high-speed camera was used to image the wave in the transition region and provide spatial information. High frequency pressure transducers were used along the combustor axis to determine wave speed. The ultimate goal was to determine the conditions required to ensure reliable re-establishment of a detonation wave in the JP-10/air aerosol mixture.  Unfortunately, the confined planar JP-10/oxygen detonations in the pre-detonator were unable to transition into unconfined spherical detonation fronts in the JP-10/air aerosol. Furthermore, the ratio of main combustor diameter to pre-detonator diameter was too large to allow re-initiation of detonation at the main combustor wall.				
<b>14. SUBJECT TERMS</b>  JP-10, Detonations, Pulse Detonation Engines, Tactical Missile Propulsion			<b>15. NUMBER OF PAGES</b> 90	
			<b>16. PRICE CODE</b>	
<b>17. SECURITY CLASSIFICATION OF REPORT</b>  Unclassified	<b>18. SECURITY CLASSIFICATION OF THIS PAGE</b>  Unclassified	<b>19. SECURITY CLASSIFICATION OF ABSTRACT</b>  Unclassified	<b>20. LIMITATION OF ABSTRACT</b>  UL	

THIS PAGE INTENTIONALLY LEFT BLANK.

Approved for public release; distribution is unlimited.

**PROPAGATION OF A TWO-PHASE DETONATION ACROSS A GEOMETRIC  
DIFFRACTION WITH COMPOSITIONAL DISCONTINUITY**

Todd A. Hofstedt  
Lieutenant, United States Navy  
B.S., United States Naval Academy, 1993

Submitted in partial fulfillment of the  
requirements for the degree of

**AERONAUTICAL AND ASTRONAUTICAL ENGINEER**

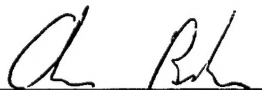
from the

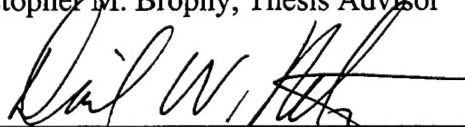
**NAVAL POSTGRADUATE SCHOOL  
June 2000**

Author:

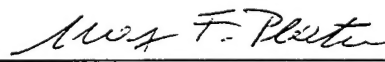
  
Todd A. Hofstedt

Approved by:

  
Christopher M. Brophy, Thesis Advisor

  
David W. Netzer, Co-Advisor

  
Raymond P. Shreeve, Second Reader

  
Maximilian Platzter, Chairman  
Department of Aeronautics and Astronautics



THIS PAGE INTENTIONALLY LEFT BLANK.

## ABSTRACT

The research program involved the modification and use of an existing pulse detonation engine (PDE) to investigate the detonability of a JP-10/air aerosol. The detonation of a JP-10 aerosol in air proved more difficult than was originally anticipated.

The use of a small JP-10/oxygen pre-detonator to provide direct initiation results in a transition region with a geometric diffraction and compositional discontinuity. Propagation of a detonation into such a region is very complex but critical to the re-establishment of the detonation wave in the JP-10/air mixture. A high-speed camera was used to image the wave in the transition region and provide spatial information. High frequency pressure transducers were used along the combustor axis to determine wave speed. The ultimate goal was to determine the conditions required to ensure reliable re-establishment of a detonation wave in the JP-10/air aerosol mixture.

Unfortunately, the confined planar JP-10/oxygen detonations in the pre-detonator were unable to transition into unconfined spherical detonation fronts in the JP-10/air aerosol. Furthermore, the ratio of main combustor diameter to pre-detonator diameter was too large to allow re-initiation of detonation at the main combustor wall.

THIS PAGE INTENTIONALLY LEFT BLANK.

## TABLE OF CONTENTS

I.	INTRODUCTION.....	1
A.	PURPOSE.....	1
B.	BACKGROUND .....	1
1.	PDE Operation .....	1
2.	Initiation of Detonation .....	4
II.	DETONATION THEORY .....	7
A.	DETONATIONS, DEFLAGRATIONS, AND EXPLOSIONS.....	7
B.	THE HUGONIOT CURVE .....	7
C.	DETONATION WAVE STRUCTURE .....	11
1.	ZND Model .....	11
2.	Cellular Structure.....	13
D.	PROPAGATION OF A DETONATION WAVE .....	17
1.	Geometric Diffraction.....	17
2.	Compositional Discontinuity.....	22
III.	PDE THERMODYNAMICS .....	25
A.	CYCLE ANALYSIS .....	25
B.	THERMAL EFFICIENCY .....	29
IV.	MATERIALS AND EQUIPMENT .....	33
A.	JP-10.....	33
B.	COMBUSTOR TUBES .....	34
C.	ATOMIZERS .....	36
D.	VALVES .....	36
E.	IGNITION SYSTEM.....	37
F.	PRESSURE TRANSDUCERS.....	37
G.	CAMERA.....	37
H.	SOFTWARE.....	37
V.	FLOW CHARACTERIZATION .....	39
A.	ATOMIZER CHARACTERIZATION .....	39
1.	Particle Distribution .....	39
2.	Flow Rates.....	43
a.	Fuel Mass Flow Rate .....	43
b.	Oxygen Mass Flow Rate .....	45
B.	EQUIVALENCE RATIO.....	46
1.	Pre-Detonator .....	46
2.	Main Combustor .....	47
VI.	RESULTS .....	51
A.	TESTING.....	51
B.	FAILURE THEORIES.....	57

<b>VII. CONCLUSION.....</b>	<b>63</b>
<b>A. SUMMARY.....</b>	<b>63</b>
<b>B. RECOMMENDATIONS .....</b>	<b>63</b>
 <b>APPENDIX HARDWARE.....</b>	 <b>65</b>
 <b>LIST OF REFERENCES .....</b>	 <b>69</b>
 <b>INITIAL DISTRIBUTION LIST .....</b>	 <b>71</b>

## LIST OF FIGURES

Figure 1.	Pressure Profile within a PDE from Ref. [3].....	2
Figure 2.	PDE Operating Cycle from Ref. [3].....	2
Figure 3.	Hugoniot Curve from Ref. [7].....	8
Figure 4.	Variation of Physical Properties through a Detonation from Ref. [7].....	11
Figure 5.	ZND Model on Hugoniot Curve from Ref. [7]. ....	12
Figure 6.	Detonation Fish-Scale Pattern from Ref. [5].....	13
Figure 7.	Axial View of Detonation Front from Ref. [5]. ....	14
Figure 8.	Double Mach Reflection of Transverse Wave from Ref. [5]. ....	14
Figure 9.	Different Ignition Regions within a Detonation Cell from Ref. [8].....	16
Figure 10.	Detonation Diffraction into Unconfined Volume from Ref. [12]. ....	18
Figure 11.	Re-Initiation in Tube with Yielding Walls from Ref. [11]. ....	20
Figure 12.	Detonation Diffraction in a Cone from Ref. [13].....	21
Figure 13.	Critical Diameter for Transmission through a Cone from Ref. [13]. ....	22
Figure 14.	Constant Pressure Combustion Cycle. ....	26
Figure 15.	Chapman-Jouguet Detonation Cycle. ....	27
Figure 16.	Cycle Comparison. ....	28
Figure 17.	Fuel Injection Element from Ref. [18]. ....	36
Figure 18.	Facility Control Layout. ....	38
Figure 19.	Phase Doppler Particle Analyzer System Layout. ....	39
Figure 20.	Droplet Sauter Mean Diameter as a Function of Pressure. ....	40
Figure 21.	Atomizer with Acrylic Extension from Ref. [19]. ....	41
Figure 22.	Droplet SMD with 5-inch Tube as a Function of Pressure. ....	42
Figure 23.	Droplet SMD with 10-inch Tube as a Function of Pressure. ....	42
Figure 24.	Atomizer Fuel Mass Flow Rate.....	44
Figure 25.	Atomizer Oxygen Mass Flow Rate. ....	46
Figure 26.	Pre-Detonator Equivalence Ratio.....	47
Figure 27.	Main Combustor Equivalence Ratio (100 psig Main Air). ....	49
Figure 28.	Main Combustor Equivalence Ratio (150 psig Main Air). ....	49
Figure 29.	PDE Test Timeline. ....	52
Figure 30.	Failed Detonation. ....	55
Figure 31.	Detonation Propagating from Pre-Detonator into Main Combustor. ....	56
Figure 32.	Shattered Quartz Section.....	57
Figure 33.	Fuel Vaporization behind the Detonation Front from Ref. [21]. ....	60

THIS PAGE INTENTIONALLY LEFT BLANK.

## LIST OF TABLES

Table 1.	Constant Pressure Combustion Cycle.....	26
Table 2.	Chapman-Jouguet Detonation Cycle. ....	28
Table 3.	Atomization-Related Properties for JP-10 and Water. ....	33
Table 4.	Combustion-Related Properties of JP-10.....	33
Table 5.	Testing Ranges of PDE Parameters. ....	53
Table 6.	Detonation Parameters by Mixture. ....	61



THIS PAGE INTENTIONALLY LEFT BLANK.

## **ACKNOWLEDGMENTS**

The author would like to acknowledge the financial support of the Office of Naval Research for enabling the purchase of the equipment used in this thesis. This work was performed under Contract N0001400WR20216.

The author would also like to thank Professor Chris Brophy for his time and effort, as well as Dr. Jose Sinibaldi and Harry Conner for all their work to support this project. Finally, the author wishes to express his appreciation for the patience and understanding of his wife, Elizabeth, whose support both facilitated and sustained this endeavour.

THIS PAGE INTENTIONALLY LEFT BLANK.

## **I. INTRODUCTION**

### **A. PURPOSE**

This investigation was conducted as part of the Office of Naval Research program for fundamental research into pulse detonation engines (PDEs). During the past year, our goal was to determine the effects of fuel distribution on detonation wave stability and velocity in a JP-10/air aerosol. Testing apparatus consisted of a 1.5625-inch inner-diameter tube, or pre-detonator, surrounded by four similar fuel/air tubes, all of which opened into a 5.25-inch inner-diameter tube, or main combustor. (See Chapter IV and the Appendix.) A JP-10/oxygen aerosol was detonated in the pre-detonator for the purpose of initiating detonation in the JP-10/air aerosol in the main combustor. A parallel goal was to minimize the oxygen requirements of the pre-detonator. Previous work at the Naval Postgraduate School included detonation studies of ethylene/air, but for volume-limited systems (e.g., tactical missiles) liquid fuels are required for a good density impulse ( $\rho I_{sp}$ ) as well as avoiding the large tank mass required to contain pressurized gases. The ultimate objective of the program is to determine the viability and design requirements of a liquid-fueled PDE for tactical missile propulsion.

### **B. BACKGROUND**

#### **1. PDE Operation**

Detonations have been studied for a variety of purposes since the 19<sup>th</sup> century. The history will not be presented here but a very good summary is given by Bauer, Dabora, and Manson [Ref. 1, 2]. In a PDE, the detonation would be used to generate high-pressure combustion products. Figure 1 illustrates the pressure profile.

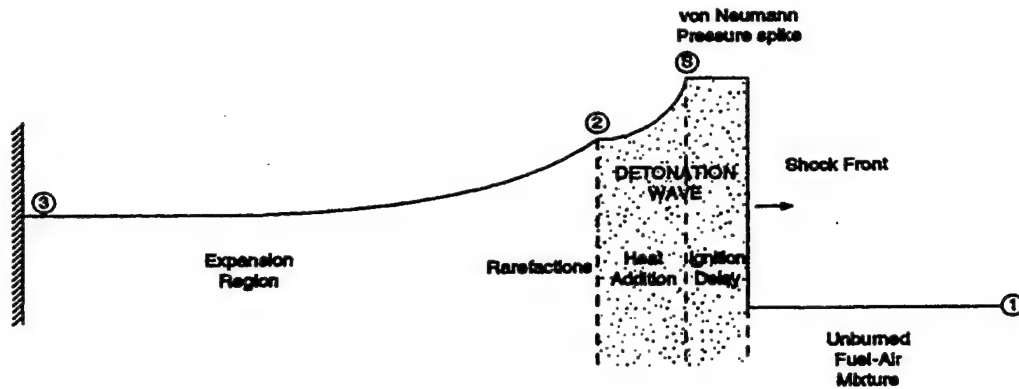


Figure 1. Pressure Profile within a PDE from Ref. [3]

The pressure against the head wall ( $P_3$ ) of the PDE combustor can be integrated over time to determine the thrust.

The operating cycle of a single-tube PDE is presented in Figure 2.

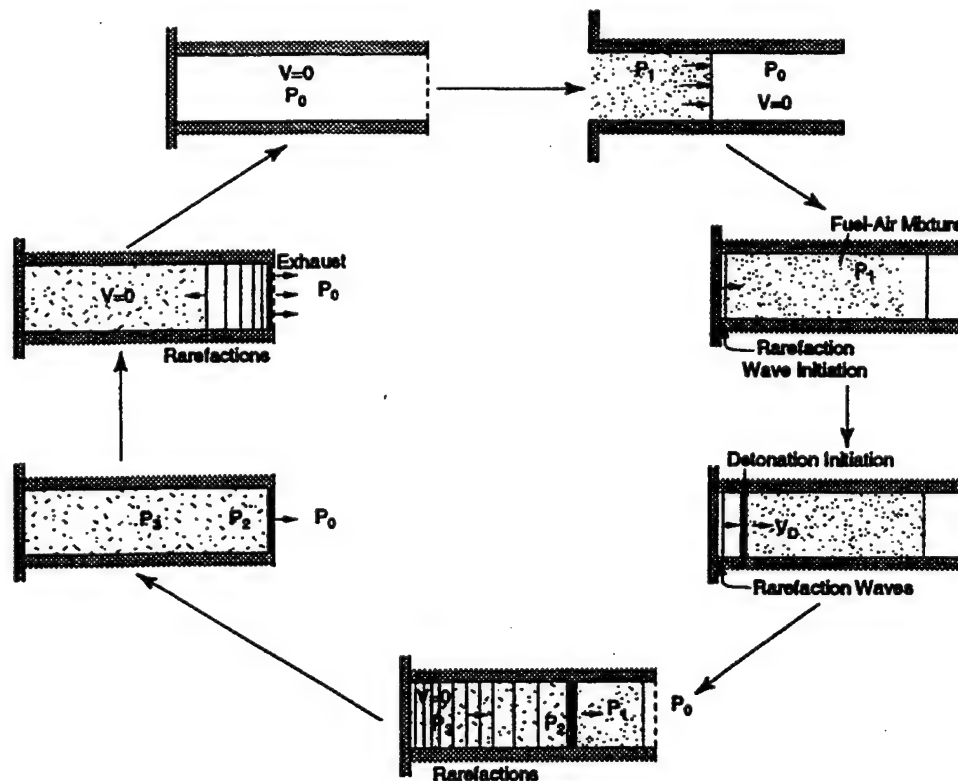


Figure 2. PDE Operating Cycle from Ref. [3]

Initially, the fuel/oxidizer mixture is injected into the combustion chamber. As soon as the valves are shut, detonation is initiated at the head end. Since the detonation products flow in the direction of the wave, and the head end boundary is closed, rarefaction waves are generated. These reduce the pressure at the head wall ( $P_3$ ) below that immediately behind the detonation ( $P_2$ ). Head wall pressure can be calculated using:

$$P_3 = \left( \frac{\gamma + 1}{2\gamma} \right)^{\frac{2\gamma}{\gamma - 1}} P_2 \quad (1)$$

where  $\gamma$  is the ratio of specific heats of the burned gases and  $P_2$  is the pressure for the Chapman-Jouguet detonation condition (described in Chapter II) [Ref. 4]. Once the detonation wave leaves the end of the tube, rarefaction waves are generated which travel towards the head end, reducing combustor pressure to ambient pressure. This serves to exhaust most of the combustion products. The cycle is then repeated. [Ref. 3]

As the operating frequency increases, the pressure on the head wall will reach a quasi-steady value. Several factors govern the maximum cycle frequency including, physical tube size, fuel and oxidizer flow rates, valve response times, control program response times, and the time required for the combustion wave to transition to a detonation. Very high detonation repeatability is also required. Since deflagration is a much slower process than detonation, a failed detonation attempt could leave a slow combustion event still occurring in the tube when the fuel/oxidizer mixture is added to begin the next cycle. This new mixture could then begin burning before the tube is ignited. Thus a single detonation failure at a high operating frequency could prevent

successful operation for several subsequent cycles. Multiple combustion tubes can also be used to increase the effective cycle frequency.

As implied above, PDEs themselves are very simple. Aside from the valving, there are no moving parts, which should make PDEs inexpensive and reliable. Although not as simple as a ramjet, the PDE has the advantage of being able to generate thrust from low subsonic through supersonic flight conditions. In addition, the cyclic nature of PDE operation makes it capable of near-instantaneous throttling over a wide thrust range.

## **2. Initiation of Detonation**

There are two modes of detonation initiation: thermal initiation (or self-ignition) and direct initiation. In thermal initiation, a tube containing an explosive mixture is ignited at the closed end. The resulting combustion products have a specific volume 5-15 times that of the reactants [Ref. 5]. This generates a series of compression waves, each one of which heats the unburned mixture to a slightly higher temperature. These higher temperatures lead to progressively higher flame speeds, which create stronger compression waves. In addition, sonic velocity in the unburned mixture is slightly higher for each successive compression wave, thereby allowing each to catch up with the initial one [Ref. 5]. Eventually the unburned gases become turbulent, accelerating the flame front even more until the compression waves coalesce into a shock of sufficient strength to ignite the unburned mixture [Ref. 5]. This reaction then supplies the energy required to sustain the shock, thus forming a detonation. This is the mode by which detonation is initiated in the pre-detonator.

The other method of initiating detonation is direct initiation, in which a strong shock is directly applied to the explosive mixture. Due to the coupling between chemical and gas dynamic processes, the sensitivity of the reactants will dictate the required strength of the shock [Ref. 5]. The pre-detonator is used to provide the strong shock for direct initiation of detonation in the main combustor. This arrangement was chosen since the deflagration-to-detonation transition distance for a JP-10/oxygen aerosol is approximately 6-8 inches under optimum conditions [Ref. 6], while for a JP-10/air aerosol it would be orders of magnitude longer [Ref. 5].



THIS PAGE INTENTIONALLY LEFT BLANK.

## II. DETONATION THEORY

### A. DETONATIONS, DEFLAGRATIONS, AND EXPLOSIONS

There are important distinctions between the terms detonation, deflagration, and explosion. A deflagration is a subsonic combustion wave, behind which the flow is accelerated with a significant reduction in density and approximately constant pressure (actually a slight reduction). By contrast, a detonation is a supersonic combustion wave, behind which the flow is decelerated with higher density and a dramatic rise in pressure. [Ref. 7]

The term explosion refers to an exothermic reaction in which the rate of heat release exceeds the rate of heat removal, thereby accelerating the reaction exponentially and creating a rapid expansion of the working fluid. The heat generation and pressure rise are very rapid, but no combustion wave is required for the process to occur. Explosions are thus a "volume reaction" vice a wave phenomenon. [Ref. 5]

### B. THE HUGONIOT CURVE

The one-dimensional mass, momentum, and energy conservation equations (for an adiabatic system in a constant area duct with no body forces) can be combined to yield the Hugoniot relation:

$$h_2 - h_1 = \frac{1}{2}(P_2 - P_1) \left( \frac{1}{\rho_1} + \frac{1}{\rho_2} \right) \quad (2)$$

where  $h$  is the total (i.e., thermal plus chemical) enthalpy,  $P$  is the pressure, and  $\rho$  is the density [Ref. 7]. Alternatively, in terms of internal energy, the Hugoniot relation can be written as:

$$e_2 - e_1 = \frac{1}{2}(P_2 + P_1) \left( \frac{1}{\rho_1} - \frac{1}{\rho_2} \right) \quad (3)$$

where  $e$  is the total internal energy [Ref. 5]. The Hugoniot curve, Figure 3, is a plot of  $P_2$  versus  $1/\rho_2$  for a given heat release.

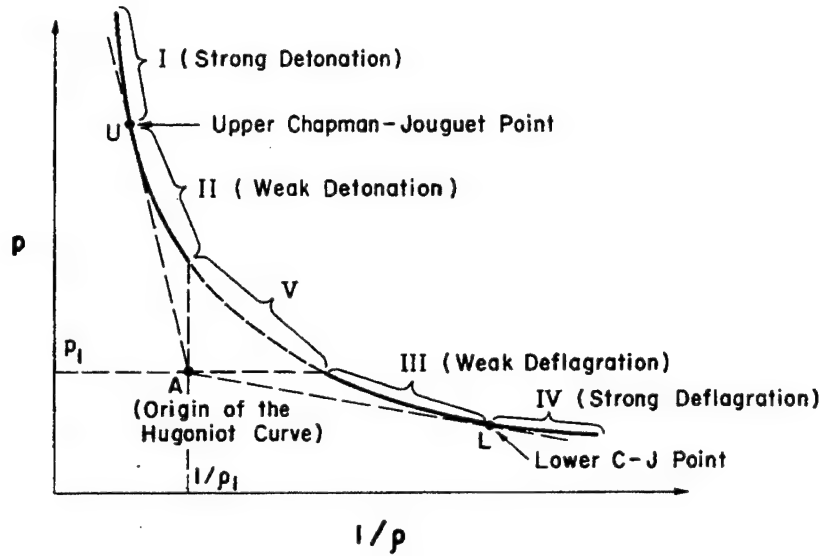


Figure 3. Hugoniot Curve from Ref. [7]

For an adiabatic process, the Hugoniot curve would pass through the origin (point A in Figure 3), representing a normal shock (upper branch) or expansion (lower branch). With heat release, the curve shifts up and to the right, with greater heat release causing a greater shift. The upper branch, then, generally indicates a supersonic combustion process (i.e., detonation) while the lower branch indicates a subsonic heat release process (i.e., deflagration).

For diabatic flow in a constant area duct, the conservation equations also lead to the Rayleigh relation:

$$\rho_1^2 u_1^2 = \frac{\frac{P_2 - P_1}{1} - \frac{P_1}{1}}{\frac{1}{\rho_1} - \frac{1}{\rho_2}} \quad (4)$$

where  $u_1$  is the velocity of the unburned gases relative to the detonation wave [Ref. 7]. In terms of Mach number, this becomes:

$$\gamma M_1^2 = \frac{\frac{P_2}{P_1} - 1}{1 - \frac{\rho_1}{\rho_2}} \quad (5)$$

where  $\gamma$  is the ratio of specific heats and  $M_1$  is the Mach number of the unburned gases relative to the detonation wave (or, alternatively, the Mach number of the detonation wave propagating into the unburned gases) [Ref. 7].

Rayleigh lines passing through the origin of the Hugoniot curve (e.g., the dashed lines in Figure 3.) serve to divide it into regions representing different physical phenomena. The points of tangency are known as the Chapman-Jouguet points, or C-J points. Since a Rayleigh line with a less negative slope could not pass through both the detonation branch of the Hugoniot curve and the origin, the upper C-J point (U) yields the minimum detonation wave speed [Ref. 7]. It can also be shown that this point corresponds to the point of minimum entropy on the Hugoniot curve [Ref. 7].

Conversely, the lower C-J point (L) results in the maximum deflagration wave speed and the maximum entropy [Ref. 7]. At both C-J points, it can be shown that the burned gases travel at sonic velocity (i.e.,  $M_{2,U} = M_{2,L} = 1$ ) [Ref. 5]. However, in a detonation, the burned gases flow in the same direction as the wave, while in a deflagration they flow away from it [Ref. 7].

The upper C-J point also represents the only steady-state solution in the detonation branch of the Hugoniot curve. Region I of the Hugoniot curve (using the notation from Figure 3) is called the strong detonation region. Here  $P_2 > P_U$  so  $u_2 < u_{2,U}$  [Ref. 5]. Since  $M_2 < 1$ , any rarefaction wave, such as could be caused by heat loss, turbulence, or friction, would overtake the detonation front and reduce its pressure [Ref. 5]. This would shift the detonation down the Hugoniot curve until it reached point U, at which point  $M_2 = 1$  and rarefaction waves would no longer be able to catch up with the detonation front. Thus the wave would reach a steady-state condition.

Since a detonation is fundamentally a shock that induces chemical energy release, the process initially moves upward along the shock Hugoniot from the origin and then (with heat release) travels down along a Rayleigh line to the final Hugoniot [Ref. 5]. A Rayleigh line that passes through both the origin and Region II must also pass through Region I. To travel down a Rayleigh line from Region I to Region II would require additional heat release. However, additional shock-induced heat release would simply shift the resulting Hugoniot curve up and to the right, with the final state in Region I of the new Hugoniot but approaching point U. Thus Region II is not theoretically attainable. (However, extremely fast chemical kinetics combined with physical processes that do not quite follow the idealized model above could make weak detonation waves possible [Ref. 7].)

Region III, weak deflagration, is simply the combustion phenomena commonly observed under most conditions. Region IV, strong deflagration, would require  $M_2 > 1$ . Since heat addition to a constant-area flow cannot accelerate the flow from subsonic to

supersonic, solutions in this region are not possible. Finally, in Region V,  $P_2 > P_1$  and  $1/\rho_2 > 1/\rho_1$ . From the Rayleigh relation (Equation 4),  $u_1$  would be imaginary, so solutions here are not physically possible either.

## C. DETONATION WAVE STRUCTURE

### 1. ZND Model

The classic one-dimensional detonation wave model was determined independently by Zel'dovich, von Neumann, and Döring. According to this model, the detonation wave consists of a planar shock wave followed by a chemical reaction region. The shock compresses and heats the combustible mixture which, after an induction period, reacts. The reaction actually begins immediately but for reactions that follow Arrhenius' Law and have a relatively large activation energy – such as hydrocarbon oxidation – the fraction of material reacted changes very little initially but then proceeds to completion at a very high rate [Ref. 5]. This chemical reaction then provides the energy to sustain the shock wave. The variation of physical properties through the detonation wave is shown in Figure 4.

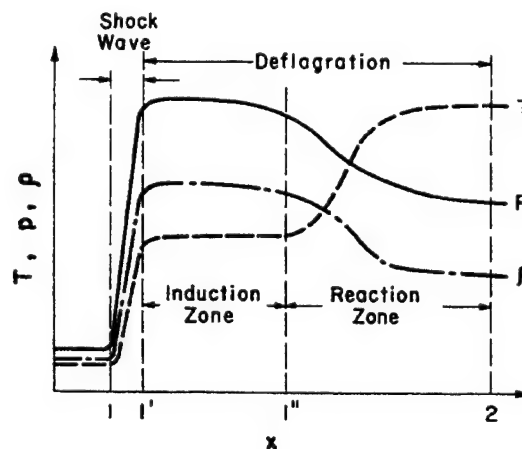


Figure 4. Variation of Physical Properties through a Detonation from Ref. [7]

A plot of the ZND model on a Hugoniot Curve is given in Figure 5.

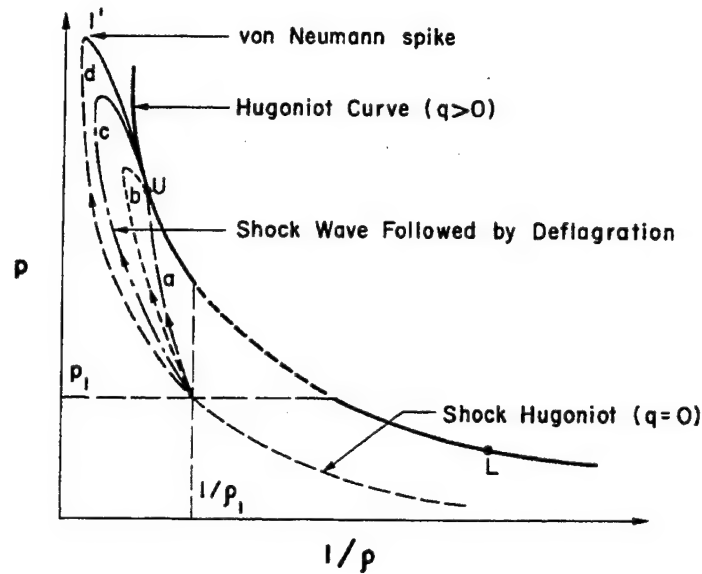


Figure 5. ZND Model on Hugoniot Curve from Ref. [7]

The particular path followed (a, b, c, or d, from Figure 5) depends upon the reactants being detonated. The progression from a through d represents progressively slower chemical kinetics [Ref. 7]. Path a represents the unattainable limit in which reaction occurs everywhere through the detonation wave. This would require the reaction to begin at the same instant as – and proceed in parallel with – the pressure and temperature rise (i.e., exhibiting no causal relationship). Approaching the other extreme (path d), the progressively slower chemical kinetics result in progressively larger pressure spikes. This spike is short in duration and rapidly disappears as the chemical reaction begins. The peak pressure in the detonation wave is referred to as the von Neumann spike [Ref. 7].

## 2. Cellular Structure

In an actual detonation wave, the ZND structure described above is hydrodynamically unstable and only observed under transient conditions. [Ref. 7, 8] The chemical reactions behind the detonation do not just direct energy toward the detonation front, but also transversely. This forms transverse waves, which give detonations a complex three-dimensional structure. This structure is cellular in nature and appears as a fish-scale pattern on smoked foil. Figure 6 provides an example of this pattern and Figure 7 illustrates the cellular structure in an axial view of a detonation front.

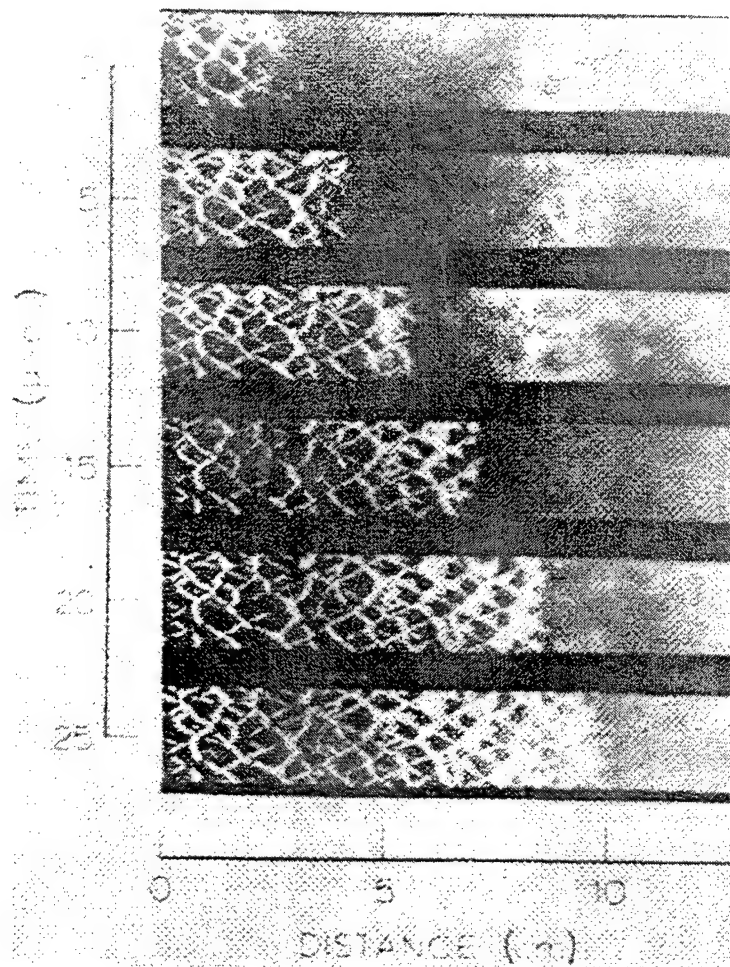


Figure 6. Detonation Fish-Scale Pattern from Ref. [5]



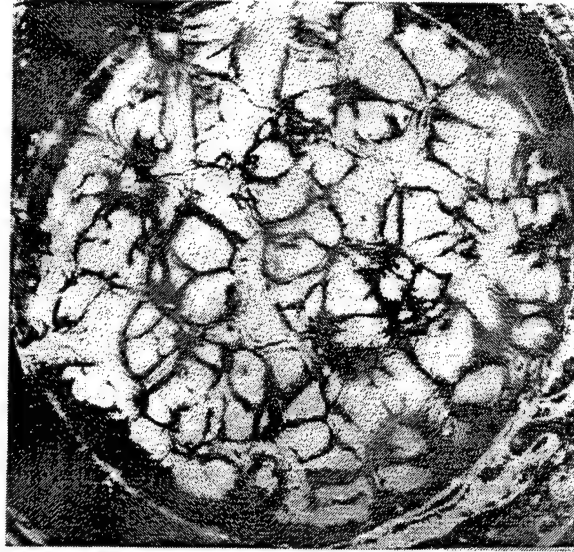


Figure 7. Axial View of Detonation Front from Ref. [5]

The fish-scale pattern indicates the path of triple points in the transverse waves. There are actually two triple points (A and B in Figure 8), forming a double Mach reflection. [Ref. 5]

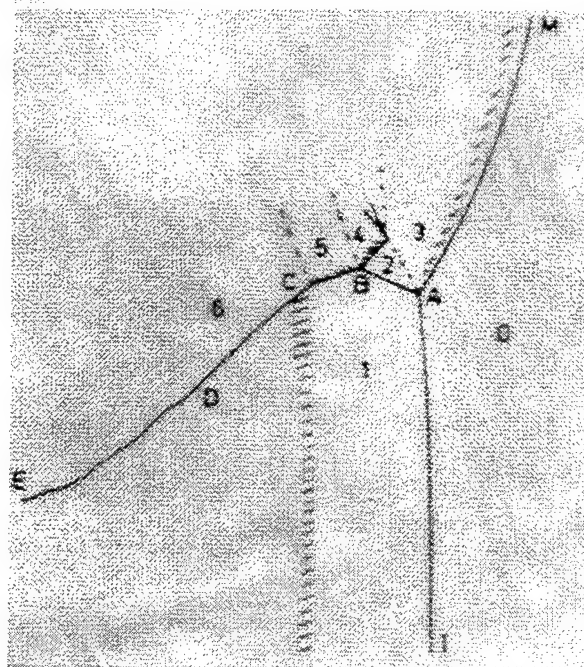


Figure 8. Double Mach Reflection of Transverse Wave from Ref. [5]

In Figure 8, the detonation is propagating to the right. Segment IA is the incident shock, MA is the Mach stem, and AB is the reflected shock. The hatched lines show the reaction front and the dash-dot lines are slip lines. Cell length ( $L_c$ ), defined as the cell dimension along the axis of detonation propagation, is determined by the length of segment AD. Cell size ( $\lambda$ ) (also referred to as cell width or cell diameter) is the cell dimension perpendicular to the direction of propagation and is governed by the length of segment BC. Segment ABCDE forms the transverse wave, propagating downward at approximately sonic speed in the burned gases. [Ref. 5]

Lee (as quoted in Reference 5) describes the cyclic motion as follows:

Starting at the apex of the cell at A, the detonation shock front is highly overdriven, propagating at about 1.6 times the equilibrium Chapman-Jouguet detonation velocity. Toward the end of the cell at D, the shock has decayed to about 0.6 times the Chapman-Jouguet velocity before it is impulsively accelerated back to its highly overdriven state when the transverse waves collide to start the cycle again. For the first half of the propagation from A to BC, the wave serves as the Mach stem to the incident shocks of the adjacent cells. During the second half from BC to D, the wave then becomes the incident shock to the Mach stems of the neighboring cells.

The resulting average wave velocity is very close to the equilibrium Chapman-Jouguet value [Ref. 5].

The chemical reactions are essentially completed within one cell length, and

$$\lambda \approx 0.6L_c \quad (6)$$

Therefore, as originally suggested by Shchelkin and Troshin (as discussed in Reference 9), cell size becomes an indication of the induction zone thickness and thus the chemical induction time. Accordingly, cell size increases as the sensitivity of the mixture decreases. [Ref. 5]

Unfortunately, cell size itself is not always clearly defined. When the cell size is small (i.e., sensitive mixtures), cell structure is usually quite distinct [Ref. 10]. However, as mixture sensitivity decreases, multiple instability modes appear in the transverse waves [Ref. 10]. These interact nonlinearly to create an irregular detonation structure [Ref. 10]. Within this structure, pressures and temperatures can differ by several times, causing induction time to vary by two to three orders of magnitude [Ref. 8]. Consequently, only the mixture in the first half of the cell is directly ignited by the detonation shock wave (Region one in Figure 9), and with the hottest points being ignited almost without delay [Ref. 8]. Figure 9 identifies by region the different ignition delays within a cell of an upward propagating detonation.

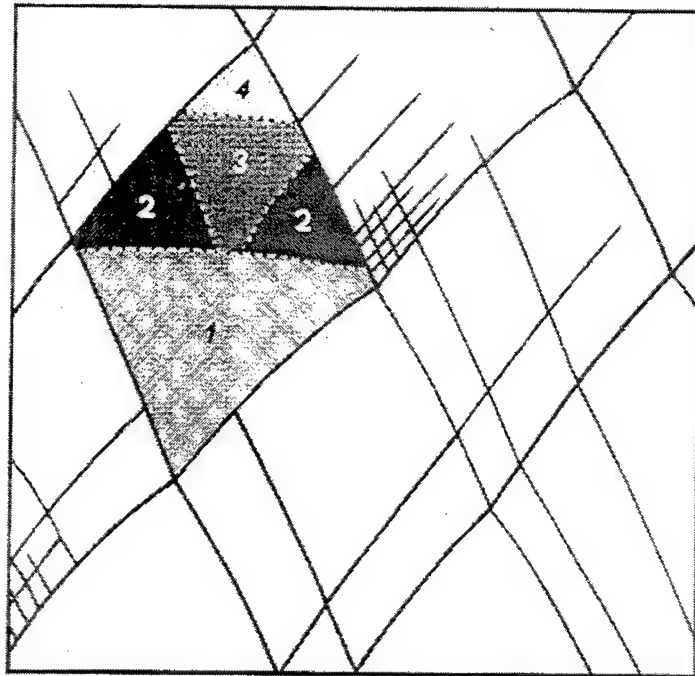


Figure 9. Different Ignition Regions within a Detonation Cell from Ref. [8]

Region two requires the additional compression of a transverse wave for ignition, and Region three requires still another shock compression [Ref. 8]. Region four, which only exists in a portion of the cells, may not react until much later [Ref. 8]. Thus, the effective reaction zone is many times larger than that predicted by the ZND model. This complex structure makes determination of a dominant mode difficult, thereby limiting the utility of empirical laws based on cell size [Ref. 10].

#### **D. PROPAGATION OF A DETONATION WAVE**

##### **1. Geometric Diffraction**

Cell size strongly affects the propagation of a detonation through a geometric diffraction. When a detonation leaves a constant-area tube and enters an unconfined region containing the same mixture, rarefaction waves propagate radially inward. This reduces the mixture temperature, thereby increasing chemical induction time. The resulting delay may decouple the reaction zone from the shock. The original tube diameter must be large enough to allow transverse wave interactions to establish a spherical detonation front before the original detonation core is quenched. Otherwise, the source of the transverse waves is removed, thus preventing direct re-initiation of the detonation and leaving the reaction to propagate as a deflagration. Since the detonation core itself propagates at approximately twice sonic velocity in the burned gases, it travels a distance of approximately one tube diameter before being quenched by the radially propagating rarefaction waves [Ref. 11]. Thus, re-initiation of the detonation must occur within this distance [Ref. 9]. Figure 10 shows a successful transition from confined planar to unconfined spherical detonation.

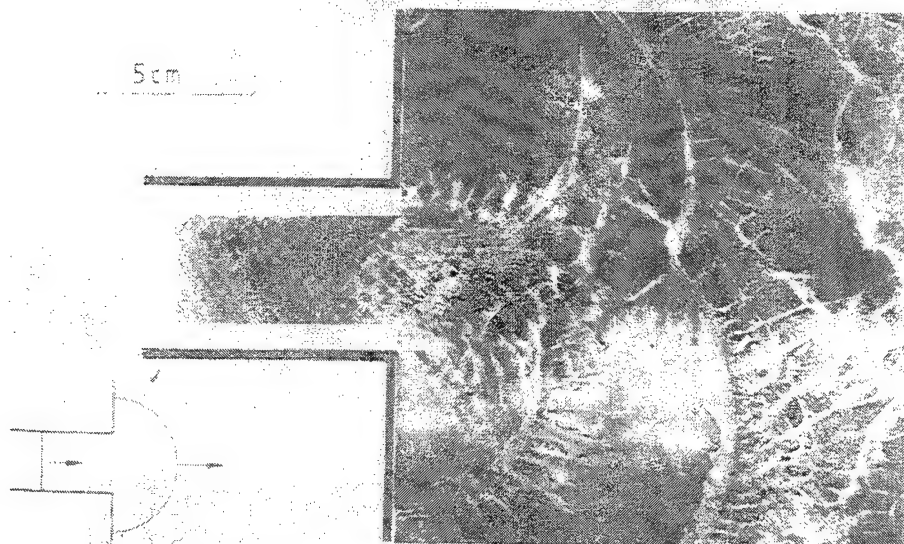


Figure 10. Detonation Diffraction into Unconfined Volume from Ref. [12]

The minimum tube diameter required for a detonation to transition from confined planar to unconfined spherical propagation in the same mixture is known as the critical tube diameter ( $d_c$ ) [Ref. 5, 9]. According to the empirical law of Soloukhin and Mitrofanov (as discussed in Reference 9), and supported by observations of other researchers [Ref. 5],

$$d_c \approx 13\lambda \quad (7)$$

The mechanism governing the expansion of a detonation front is the generation of additional transverse waves, which leads to the creation of very small new cells. Transverse waves may be initiated by small random perturbations in the detonation wave or by the smallest cells within some of the largest cells in an irregular structure. In the latter mechanism, cells in which the induction length exceeds the critical detonation value

can actually generate a transverse C-J detonation if ignited by the collision of two transverse waves. These transverse detonations (as well as major transverse wave collisions) generate convex overdriven detonation fronts in the adjacent unburned mixture. This overdriven front initially consists of very fine cells, which then grow to form the main structure as the wave returns to the C-J condition. [Ref. 8]

Less extreme forms of geometric diffraction can facilitate transmission of the detonation by providing preferential locations for re-initiation. Murray and Lee [Ref. 11] report on a study in which detonations propagated from a rigid tube into a yielding tube of the same diameter. By varying the thickness of the yielding wall, they could control the strength of the lateral rarefaction wave, thereby allowing re-initiation in less sensitive mixtures than would be required for transmission to an unconfined medium. Here the yielding wall becomes a source of reignition nuclei for the re-initiation of detonation. The process is illustrated in Figure 11.

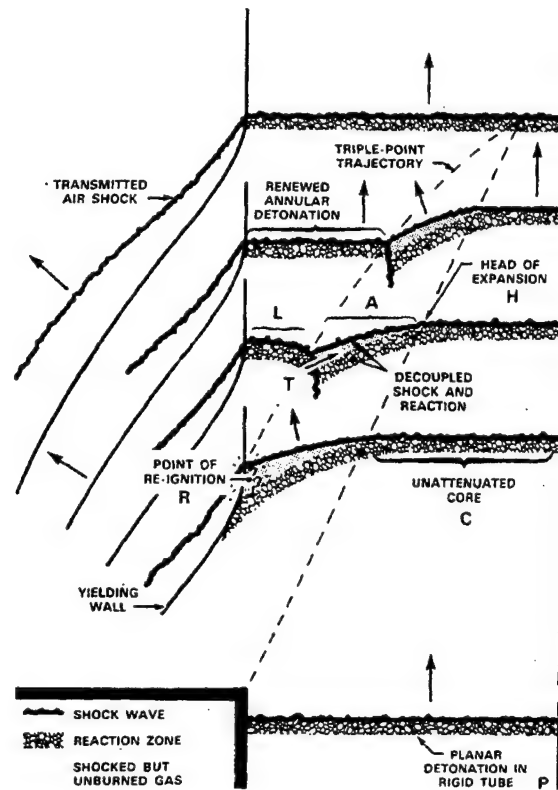


Figure 11. Re-initiation in Tube with Yielding Walls from Ref. [11]

As with propagation into an unconfined region, the detonation core is still quenched at a distance approximately one tube diameter from the end of the rigid tube. Here, however, an annular detonation forms near the wall behind the detonation core. Although the core detonation is required to generate the transverse waves for re-ignition, once detonation near the wall is initiated it will propagate circumferentially and then radially until a planar detonation front is reformed, even if the initial core detonation has already been quenched. [Ref. 11]

Murray and Lee [Ref. 11] give four possible causes for the preferential formation of re-ignition nuclei near the wall. Quoting Reference 11:

- 1) it may be induced by reflection of transverse wave remnants from the wall;
- 2) a thicker layer of shocked but unreacted gas exists near the wall; thus, possibly satisfying a minimum volume prerequisite for reignition;
- 3) a higher temperature may exist near the wall due to the presence of "x" shaped compression waves behind the slightly curved shock front;
- 4) small ripples or other irregularities in the polyethylene surface may give rise to localized shock reflections and thus hot spots.

Another variation is given by Borisov et al [Ref. 13]. By means of a process similar to the above, detonation diffraction into cones of less than 60 degrees also causes reignition at the boundary. This allows the use of detonation tubes with diameters smaller than the critical diameter if a cone is used to assist transmission. Figure 12 illustrates the arrangement.

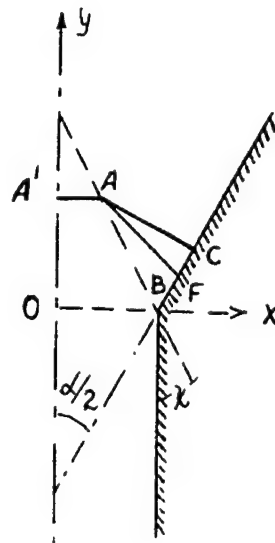


Figure 12. Detonation Diffraction in a Cone from Ref. [13]

In Figure 12,  $\alpha$  is the cone angle, segment AA' is the core detonation, segment AC is the lateral oblique shock wave, segment AB shows the radial extent of the core detonation at each axial position, and segment AF shows the boundary between the



compressed but unburned mixture and the reaction zone. Under critical conditions, detonation is reinitiated at the wall just as the core detonation is quenched (i.e., point A reaches the axis). At that point, by definition, the total energy in region ACF must be sufficient to reinitiate detonation [Ref. 13]. The volume requirements for initiation energy, however, are but one of the considerations. For cone angles greater than 60 degrees, the lateral oblique shock is too weak (leading to excessively long ignition delays) to support re-initiation of the detonation at the boundary [Ref. 13]. Figure 13 shows the required diameter for detonation transmission as a function of cone angle. The filled circles represent successful re-initiations and the open circles represent failures.

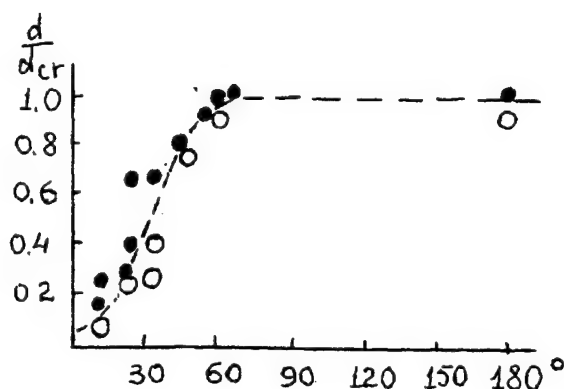


Figure 13. Critical Diameter for Transmission through a Cone from Ref. [13]

## 2. Compositional Discontinuity

Desbordes and Lannoy [Ref. 12] examined detonation propagation with a step-drop to a leaner (i.e., less reactive) mixture. Since the C-J pressure, detonation velocity, etc., are lower in the second mixture (B), a detonation propagating at C-J conditions in the initial mixture (A) enters mixture B overdriven. This results in a smaller initial cell size in mixture B, thereby reducing the critical tube diameter. Expectedly, as the

sensitivity of mixture B is reduced, its critical tube diameter increases. However, the ratio of its critical diameter to its critical diameter under C-J conditions actually goes down. (If the detonation is not overdriven by more than 20%, Equation 7 still applies.) This allows transmission from a smaller tube into an unconfined volume. As the detonation propagates through B, cell size grows monotonically until C-J conditions are reached. [Ref. 12]

When the detonation in A reaches mixture B, there is a slight delay (which increases with C-J cell size in B) in the transmission of the detonation [Ref 12]. In 1963, Shchelkin (as discussed in Reference 11) proposed that if the chemical induction time increases by an amount on the order of itself, the periodic cellular mechanism will break down and the required coupling of chemical and gas dynamic processes will not resume. This theory is supported by Murray and Lee observations of cell size approximately doubling prior to recovery from near-critical perturbations [Ref. 11].

THIS PAGE INTENTIONALLY LEFT BLANK.

### III. PDE THERMODYNAMICS

#### A. CYCLE ANALYSIS

Most current chemical propulsion systems are based on constant pressure combustion processes. This becomes a standard with which to compare the PDE, which, using a C-J detonation, is closer to a constant volume combustion process. The two key differences are the amount of heat addition (based on differences in the method of combustion) and whether that heat is added along an isobar or a Rayleigh line.

The two cycles were compared for a stoichiometric mixture of JP-10 and air (i.e., one mole of JP-10 to 14 moles of oxygen and 52.64 moles of nitrogen). As a basis for comparison, state zero was taken to be 0.1 atmospheres (representing ambient pressure under potential flight conditions). Isentropic compression to 1.0 atmosphere and 300 K yielded chamber conditions (under both flight and laboratory conditions) at state one. The Thermo-Chemical Equilibrium Program (TEP) [Ref. 14] was used to determine the conditions at state two based on the respective cycle. The expansion process from state two to state four was taken to be isentropic and the ideal gas law was assumed to hold throughout. The parameters from TEP were the frozen equilibrium values and recombination of radical species was ignored.

The constant pressure combustion cycle, or Brayton cycle, is illustrated in Figure 14 and the physical properties at each state are given in Table 1.

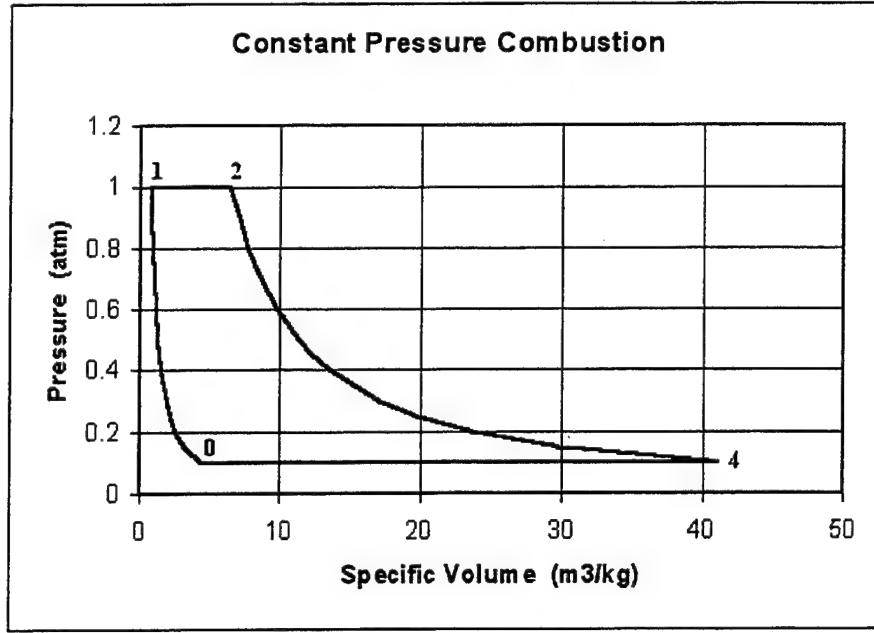


Figure 14. Constant Pressure Combustion Cycle

STATE	Pressure (atm)	Temperature (K)	Specific Volume (m <sup>3</sup> /kg)
0	0.1	165	4.447
1	1.0	300	0.809
2	1.0	2293	6.536
4	0.1	1444	41.100

Table 1. Constant Pressure Combustion Cycle

Specific volume at state one ( $v_1$ ) was found using the known inputs and the ideal gas law:

$$Pv = \frac{\bar{R}}{M} T \quad (8)$$

where  $P$  is the pressure,  $v$  is the specific volume,  $\bar{R}$  is the universal gas constant ( $8314 \text{ J/kgmol K}$ ),  $M$  is the molecular mass ( $30.4246 \text{ kg/kgmol}$  at states zero and one), and

T is the temperature. Since the compression from zero to one is isentropic,  $v_0$  was calculated using:

$$P_0 v_0^\gamma = P_1 v_1^\gamma = C \quad (9)$$

where  $\gamma$  is the specific heat ratio (initially 1.3513, from TEP) and C is a constant.

Temperature at state zero was then found using the ideal gas law (Equation 8). The properties at state four were determined in analogous fashion, using the post-combustion ratio of specific heats (1.2523) and molecular mass ( $28.832 \text{ kg/kgmol}$ ) from TEP.

The C-J detonation cycle is illustrated in Figure 15 and the physical properties at each state are given in Table 2.

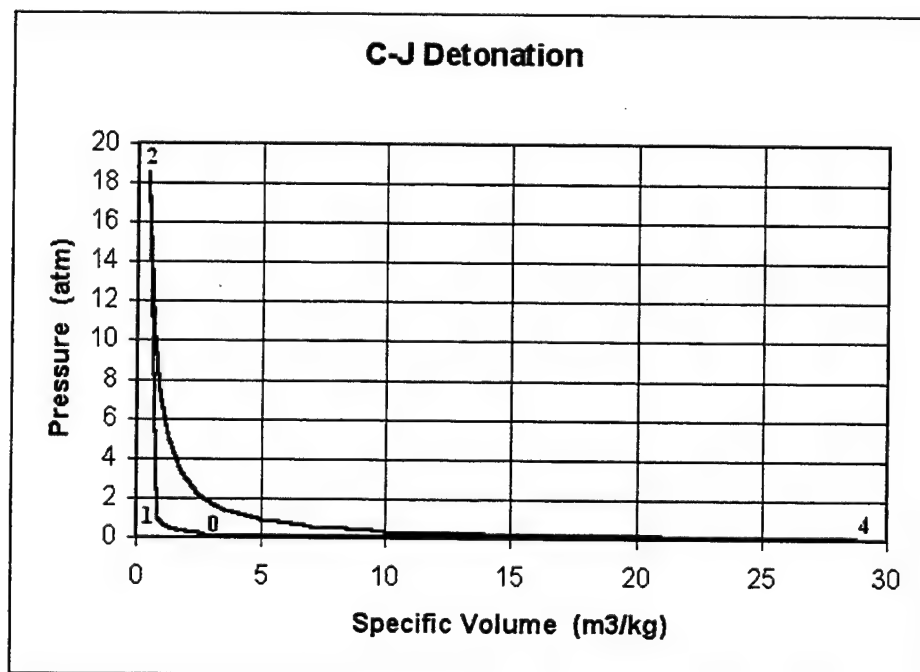


Figure 15. Chapman-Jouguet Detonation Cycle

STATE	Pressure (atm)	Temperature (K)	Specific Volume (m <sup>3</sup> /kg)
0	0.1	165	4.447
1	1.0	300	0.809
2	18.464	2851	0.446
4	0.1	996	28.791

Table 2. Chapman-Jouguet Detonation Cycle

The state zero and one conditions are identical to those for the constant pressure combustion cycle. State two was determined by TEP and state four was calculated using Equations 8 and 9.

The results above quantify some of the differences between detonation and deflagration discussed qualitatively in Chapter II. The two cycles are plotted together in Figure 16.

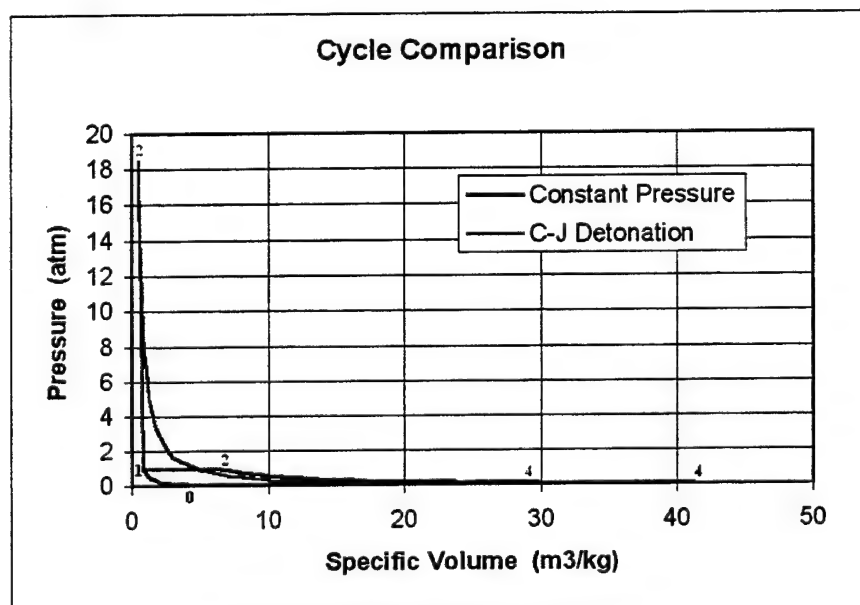


Figure 16. Cycle Comparison

Figure 16 highlights the dramatic difference between the two cycles.

Temperature is somewhat higher for the detonation (the rise is actually mitigated by the formation of additional radical species) but the real differences are in the pressure and specific volume. The detonation pressure at state two is a factor of almost 18.5 greater. In addition, while the constant pressure (deflagration) process increased the specific volume by eight times, the detonation reduced specific volume almost in half. The much larger enclosed area for the C-J detonation indicates a significant advantage in net cycle work.

## B. THERMAL EFFICIENCY

The heat released in a constant pressure combustion process (with negligible change in velocity) is simply the difference in enthalpy between the states or:

$$q_{in} = h_2 - h_1 = c_{p_2} T_2 - c_{p_1} T_1 \quad (10)$$

where  $q_{in}$  is the chemical energy released,  $h$  is the enthalpy, and  $c_p$  is the specific heat at constant pressure. The values at state two were from TEP ( $c_p$  of  $1.4315 \text{ kJ/kg K}$  at  $2293 \text{ K}$ ). The initial specific heat ( $1.0397 \text{ kJ/kg K}$ ) was calculated as the mass-weighted average of the JP-10 ( $1.60 \text{ kJ/kg K}$ ) and the air ( $1.000 \text{ kJ/kg K}$ ) at  $300 \text{ K}$  [Ref. 14]. The resulting heat release was  $2970.5 \text{ kJ/kg}$ .

Since the compression and expansion were assumed to be isentropic, the net work path integral is easily solved:

$$w_{c_p} = \oint P dv = \frac{P_1 v_1 - P_0 v_0}{1 - \gamma_1} + P_2 (v_2 - v_1) + \frac{P_4 v_4 - P_2 v_2}{1 - \gamma_2} + P_4 (v_0 - v_4) \quad (11)$$



where  $w_{cp}$  is the net work of the cycle. Using the values in Table 1, result is  $1078.1 \text{ kJ/kg}$ .

The thermal efficiency for the cycle is the ratio of net work out to heat added, or

$$\eta_{th} = \frac{w_{net}}{q_{in}} \quad (12)$$

where  $\eta_{th}$  is the thermal efficiency. For a constant pressure combustion process under these conditions, the result is 36.3 %.

The C-J detonation process inherently involves flow so more terms are required for the energy balance:

$$q_{in} = c_{p2} T_2 + \frac{u_2^2}{2} - c_{p1} T_1 - \frac{u_1^2}{2} \quad (13)$$

where  $u$  is the velocity relative to the detonation front. In this case,  $q_{in}$  refers to the total chemical energy release, which for a detonation includes energy release in the form of flow work. Since the reactants are stationary, the relative velocity at state one is simply detonation wave velocity ( $1786.6 \text{ m/s}$ ). Other state one parameters are the same as above. The values from TEP at state two for specific heat and temperature were  $1.4532 \text{ kJ/kg K}$  and  $2851 \text{ K}$ , respectively. The combustion products flow toward the detonation at sonic velocity ( $985.5 \text{ m/s}$ ) but the detonation, in this case, is travelling at  $1786.6 \text{ m/s}$ . The relative velocity at state two, then, is the difference between these. The resulting total chemical energy release is  $2556.2 \text{ kJ/kg}$ .

The net work is calculated the same as above except the C-J detonation cycle follows a Rayleigh line from state one to two instead of an isobar. Thus, the first, third, and fourth terms in Equation 11 remain the same, or:

$$w_{C-J} = w_{c_p} - P_2(v_2 - v_1) + \left( \frac{P_2 - P_1}{v_2 - v_1} \frac{1}{2} \right) (v_2^2 - v_1^2) + \left( P_2 - \frac{P_2 - P_1}{v_2 - v_1} v_2 \right) (v_2 - v_1) \quad (14)$$

Canceling like terms yields

$$w_{C-J} = w_{c_p} + \left( \frac{P_2 - P_1}{v_2 - v_1} \frac{1}{2} \right) (v_2^2 - v_1^2) - \left( \frac{P_2 - P_1}{v_2 - v_1} v_2 \right) (v_2 - v_1) \quad (15)$$

Substituting the values from Table 2 into Equations 11 and 15 gives a net cycle work of 1441.2 kJ/kg. Then, using Equation 12, the thermal efficiency is 56.4 %.

This impressive potential performance gain generates the interest in PDEs. Even with lower heat release, the C-J detonation process is able to perform more net work each cycle for the same fuel consumed. The substantially higher thermal efficiency of the C-J detonation cycle, compared to that of the Brayton cycle used in current aircraft and missile applications, could lead to dramatic reductions in specific fuel consumption. Ultimate PDE employment will depend upon the ability to couple this increase in thermal efficiency with a reasonable propulsive efficiency in a practical engine.

THIS PAGE INTENTIONALLY LEFT BLANK.

#### IV. MATERIALS AND EQUIPMENT

##### A. JP-10

JP-10 ( $C_{10}H_{16}$ ) is a high-density synthetic fuel for turbine driven tactical missiles. It is currently employed in military weapons systems, such as the Harpoon, and is approved for shipboard use. Although the fuel is not widely studied outside of government-funded research, its composition and properties are well known [Ref. 15].

Density, kinematic viscosity, and surface tension all affect the atomization of a liquid. Since the atomizers were characterized using water, a comparison of these properties for water and JP-10 is given in Table 3.

Atomization-Related Properties at 20°C	JP-10	Water
Density (g/cc)	0.936	0.9982
Kinematic Viscosity ( $mm^2/s$ )	3.30	1.004
Surface Tension (mN/m)	31.1	72.75

Table 3. Atomization-Related Properties for JP-10 and Water

Combustion-related properties of JP-10 are given in Table 4.

Combustion-Related Properties	JP-10
Vapor Pressure at 20°C (kPa)	0.31
Autoignition Temperature (°C)	245
Flash Point (°C)	53

Table 4. Combustion-Related Properties of JP-10

## B. COMBUSTOR TUBES

The pre-detonator, air arms, and main combustor are all stainless steel tubes with circular cross section. (See the Appendix.) The critical parameters for the pre-detonator are its length (long enough for deflagration-to-detonation transition) and its diameter (greater than the critical tube diameter). At the same time, the volume should be minimized to minimize oxygen requirements. At ten inches long, the pre-detonator slightly exceeds the 6-8 inches required to generate a detonation wave in a JP-10/oxygen aerosol [Ref. 6].

As indicated by Equation 7, critical tube diameter is governed by the detonation cell size, which itself is a function of the reactants. Unfortunately, a detailed study of JP-10 cell size as a function of equivalence ratio ( $\phi$ ) and nitrogen dilution ( $\beta$ , where  $\beta$  is zero for oxygen and 3.76 for air) does not exist, but efforts at the California Institute of Technology are currently underway to characterize these mixtures. Additional efforts at Stanford University and the University of California at San Diego are also currently in progress to determine the chemical kinetics of JP-10. Until that is completed, however, estimates based upon results for other hydrocarbon fuels must be used. Beeson, et al. [Ref. 16] report that increasing carbon content appears to slightly increase detonability (i.e., reduce cell size), although (with the exception of methane) the cell sizes are close enough so as to be within experimental error. Based on this, the cell size for JP-10 should be slightly smaller than that for JP-4. Figure 5 of Reference 16 gives JP-4/oxygen ( $\beta = 0$ ) cell sizes of 3 mm (for  $\phi = 1$ ) and 1.5 mm (for  $\phi = 1.5$ ). TEP calculations indicate that the highest detonation velocity for a JP-10/oxygen aerosol occurs near an

equivalence ratio of 2.0. Thus, under those conditions, the cell size should be around 1 mm, resulting in a critical tube diameter of approximately 13 mm. With an interior diameter of 1.5625 inches (or 39.7 mm), the pre-detonator should be more than adequate.

The four air arms have no particular physical or operational size requirements beyond providing enough length for good mixing. They have the same interior diameter as the pre-detonator but are 13 inches long (to simplify the atomizer piping layout at the head end).

The main combustor has an inner diameter of 5.25 inches (133.35 mm) and a variable length based on the number of segments installed. This length should be unimportant for initiation since if a detonation cannot be re-established within one pre-detonator diameter, the deflagration-to-detonation transition length would be prohibitively long [Ref. 5]. Since the pre-detonator exceeds the critical diameter for transition to an unconfined volume of the same mixture, there should be no physical limit on the maximum main combustor diameter, as long as the mixture uniformly fills that volume. In this case, however, the mixture composition changes at the point of diffraction. Nevertheless, while not strictly applicable, Equation 7 provides the only guidance currently available concerning transition to a spherical detonation front. The minimum diameter for stable detonation propagation is known as the limiting tube diameter or quench diameter ( $d^*$ ) [Ref. 9]. The applicable relation is

$$d^* \approx \frac{\lambda}{\pi} \quad (16)$$

Here, too, knowledge of the cell size is critical. From Figures 5 and 7a of Reference 16 and Figure 3 of Reference 17, the cell size for a JP-4/air ( $\beta = 3.76$ ) detonation at an

equivalence ratio of 1.0 is between about 45 and 60 mm. The cell size for JP-10/air at  $\phi = 1$  may or may not be slightly smaller. Using the worst-case JP-4/air cell size as a conservative estimate yields a limiting tube diameter of about 19 mm. This clearly should not be a problem. From an operational standpoint, the size of the main combustor should be large to maximize the thrust generated. The length, though, will be limited by fuel fill time, which is driven by the desired cycle frequency and flight conditions.

### C. ATOMIZERS

The BETE XA-F-PR200 system was selected as the atomizer due to its clean, discrete operation during transients and its ability to maintain low Sauter mean diameter (SMD or  $D_{32}$ ) droplets over a wide range of fuel delivery rates. The atomizer is depicted in Figure 17.

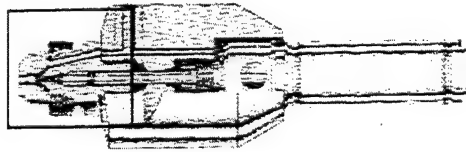


Figure 17. Fuel Injection Element from Ref. [18]

### D. VALVES

All atomization air and oxygen flow was controlled by individual Peter Paul Series 20 Model 22 9.5-watt 24-volt DC two-way solenoid valves, each with a 1/8-inch orifice (PN 22Z0573NSGM for air and PN 22Z0840NSGM for oxygen). Nitrogen pressure to open the spring-pressurized fuel shut-off cylinders in the atomizers was applied through Peter Paul Series 20 Model 23 9.5-watt 24-volt DC three-way solenoid valves, each with a 3/64-inch inlet orifice and 1/16-inch outlet orifice (PN 23Z0341NGV). Two lines supplied main air to each of the four air arms, with the flow in

each line controlled by Peter Paul Series 70 Model 72 16-watt 24-volt DC two-way solenoid valves, each with a 5/32-inch orifice. All solenoids were controlled by Crydom 6321 optically isolated relays with 100 microsecond response times.

#### **E. IGNITION SYSTEM**

The ignition system was a Unison constant 1.4 J capacitive discharge system. Thirty percent of the energy was deposited in the 40  $\mu$ s spark, for a power of 10.5 kW. The spark plug was a Champion (PN CH34168) for aircraft gas turbine ignition.

#### **F. PRESSURE TRANSDUCERS**

The pressure transducers used were Kistler piezo-electric transducers (PN 603B1) with a 2  $\mu$ s rise time. The charge output went to a Kistler charge amplifier (PN 5010B), which converted the measured pressure to a 0-5 volt output. A 540 kHz notch filter was used on each amplifier to remove the natural frequency of the transducer diaphragm.

#### **G. CAMERA**

A Princeton Instruments intensified thermo-electrically cooled charge-coupled device (ITE CCD) provided images with a resolution of 576 by 384 pixels. Shutter time was set at 500 ns. The camera controller was a Princeton Instruments ST-138 and the pulser was a Princeton Instruments PG-200.

#### **H. SOFTWARE**

Valve and ignition timing were controlled using a Visual Basic 5.0 GUI, which was also configured to monitor system pressures. The layout is presented in Figure 18.



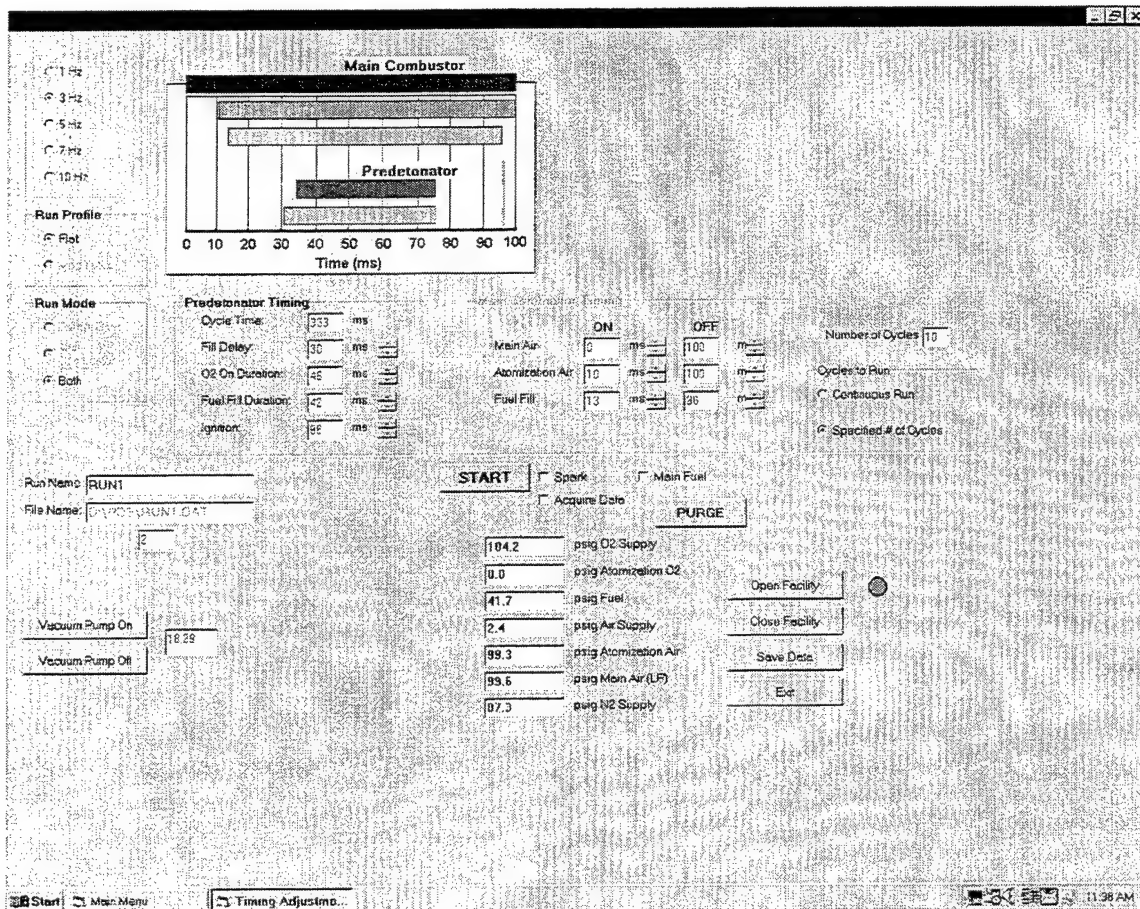


Figure 18. Facility Control Layout

## V. FLOW CHARACTERIZATION

### A. ATOMIZER CHARACTERIZATION

#### 1. Particle Distribution

An Aerometrics Phase Doppler Particle Analyzer (PDPA) system was used to determine aerosol particle size distributions. For convenience, water was used in lieu of JP-10, since its atomization characteristics have been found to be very similar [Ref. 19]. Sauter mean diameters, volumetric mean diameters, particle velocities, and other spatial statistics were obtained by the system. The argon-ion laser sample-volume was placed 7 cm (2.76 inches) downstream of the tip of the atomizer to obtain an appropriate sample with an allowable obscuration. Tests indicated that neither radial nor axial position within the spray cone had a measurable effect on droplet size, although not surprisingly particle velocity dropped appreciably with distance from the nozzle and the cone centerline. Figure 19 is a picture of the PDPA apparatus layout, showing the argon-ion laser, the optical section, and the computer for displaying and recording the data.

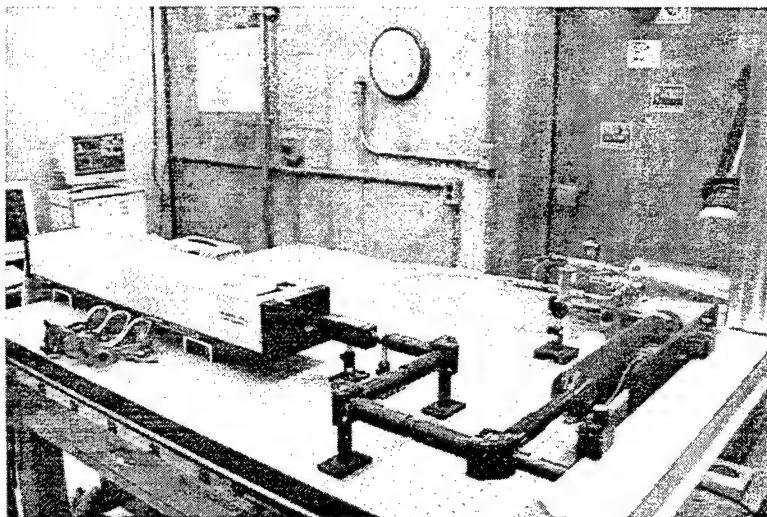


Figure 19. Phase Doppler Particle Analyzer System Layout.

The observed droplet size distributions as a function of atomization pressure are shown in Figure 20. The air and fuel pressures were limited to ranges that produced a roughly linear response, thereby allowing a linear curve fit of the data.

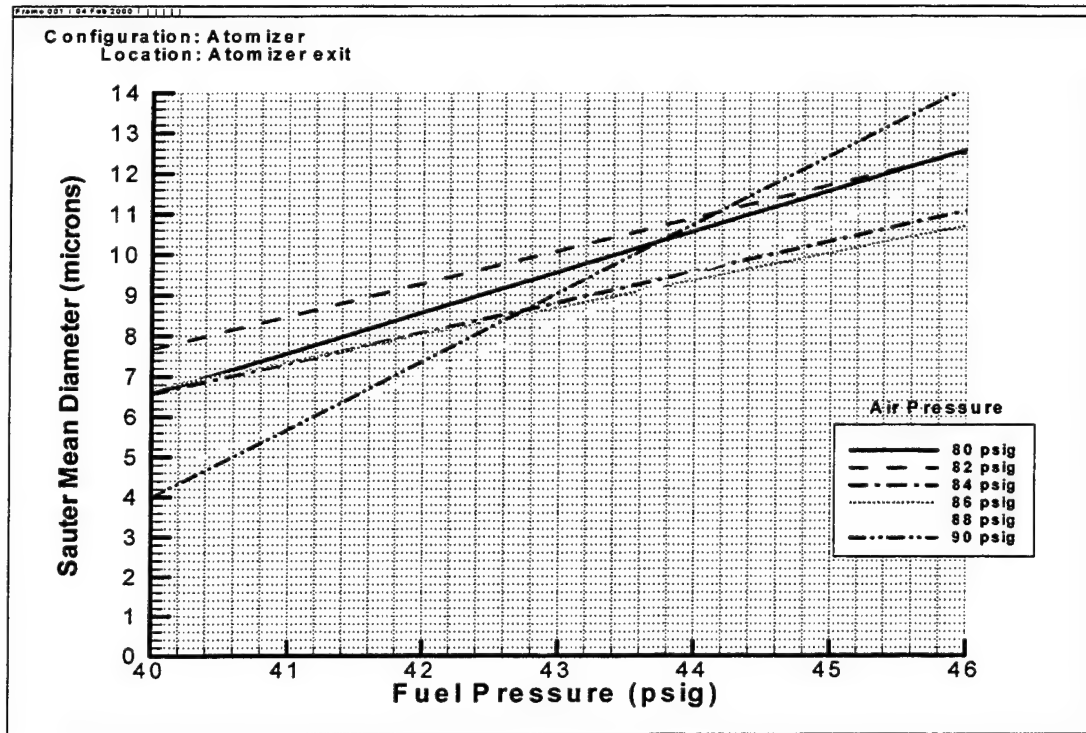


Figure 20. Droplet Sauter Mean Diameter as a Function of Pressure

Small droplet diameters are critical for the successful detonation of JP-10 in a gaseous oxidizer environment. An approach similar to the one by Tulis and Selman [Ref. 20] was taken to model droplet heating, evaporation, and oxidation. It was concluded from that analysis that droplets of approximately 10 microns in diameter and smaller could be heated and vaporized in the necessary time scales required for detonation to occur in a JP-10/oxygen mixture at ambient temperature. Figure 20 depicts the attainment of Sauter mean diameters below 10 microns for fuel pressures less than 43

psig (0.2965 MPa) and air pressures ranging from 80 psig to 90 psig (0.5516 MPa to 0.6205 MPa).

Due to the presence of a pre-detonator tube or air arms immediately following the atomizers, further flow characterization was done using 5 inch (12.7-cm) and 10 inch (25.4-cm) acrylic extensions attached to the end of the atomizer, as depicted in Figure 21.

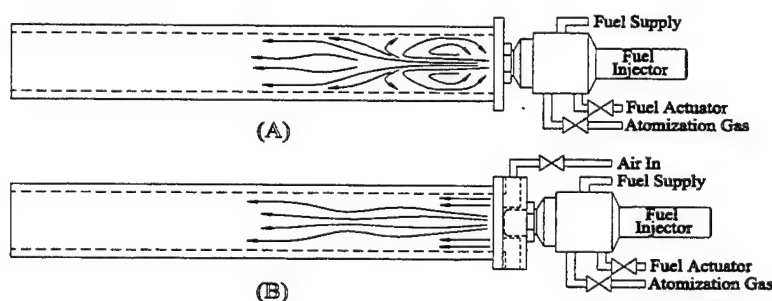


Figure 21. Atomizer with Acrylic Extension from Ref. [19]

These tubes provided an indication of the degree of uniformity, wall adhesion, and fuel agglomeration that takes place once the injector is placed inside the pre-detonator tube or an air arm. The simplest condition was the injection of a fuel/air aerosol mixture into a tube from the head end. The recirculation patterns resulted in fuel-rich conditions at the head end that promoted rapid fuel agglomeration. The flow field observed for this setup is depicted in Figure 21 (A). The flow field observed for the air arm configuration, depicted in Figure 21 (B), enabled a specified fuel-to-oxidizer ratio to be loaded with minimal wall agglomeration. Consequently, this configuration allowed a wider range of equivalence ratios to be analyzed. Figures 22 and 23 depict the SMDs attained at the exit of the 5 and 10 inch acrylic extensions, respectively. In both configurations, the minimum SMD attained was approximately 10 microns for a fuel

pressure of 40 psi (0.2758 MPa) and an air pressure of 88 psi (0.6067 MPa), with SMD ranging from 10-15 microns for all fuel/air pressure ratios.

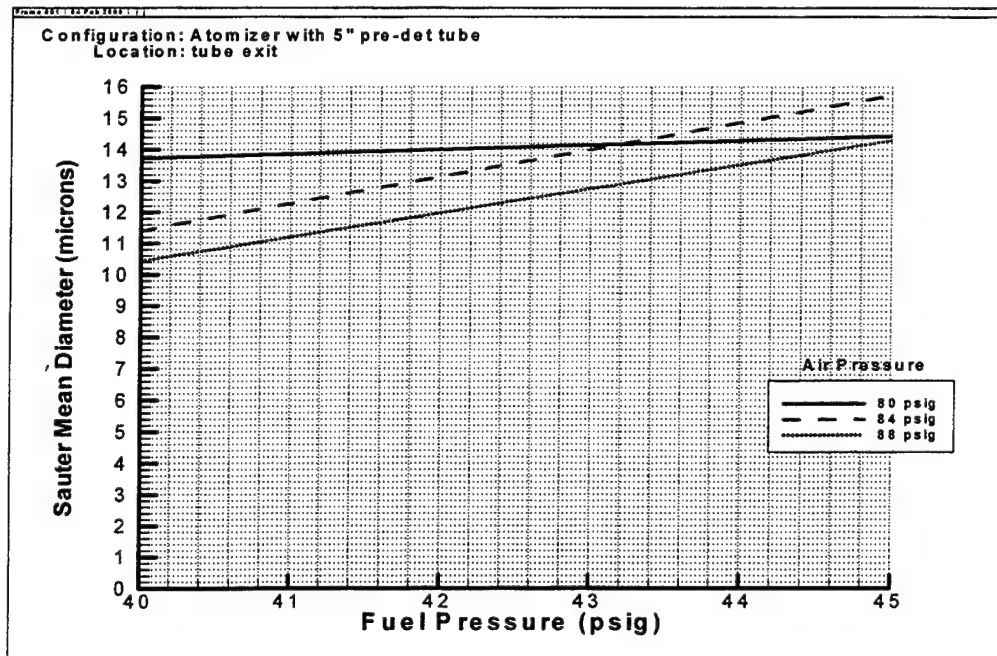


Figure 22. Droplet SMD with 5-inch Tube as a Function of Pressure

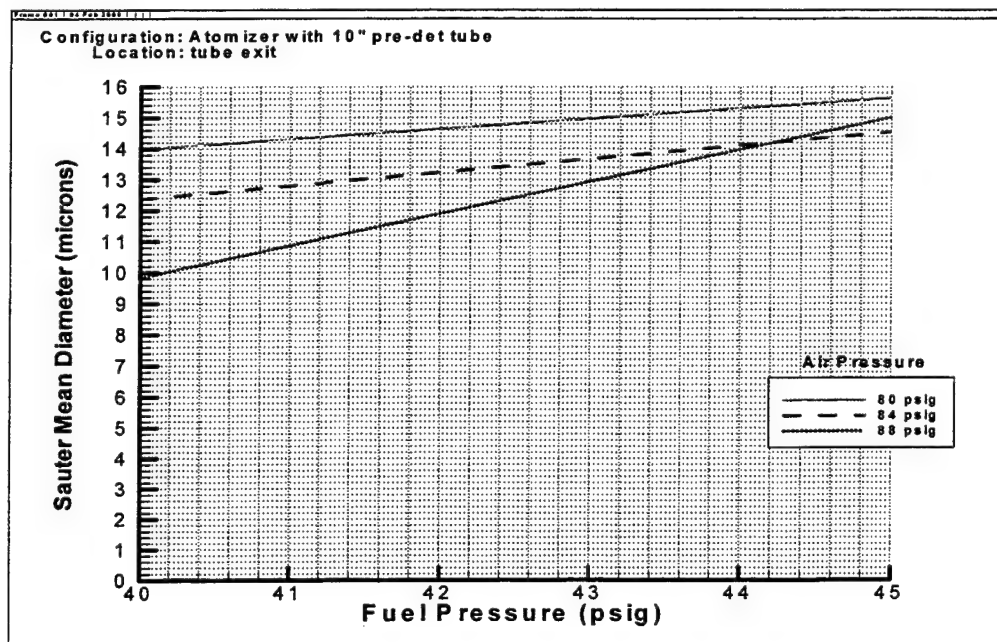


Figure 23. Droplet SMD with 10-inch Tube as a Function of Pressure

## 2. Flow Rates

### *a. Fuel Mass Flow Rate*

Mass flow rate of liquid through the atomizer was determined using a pressurized column of water. The nitrogen pressurization system was the same as that used for the fuel. Nitrogen pressure was varied from 39 psig to 45 psig in 2-psi increments. Atomization oxygen pressure was varied from approximately 80 to 90 psig at each nitrogen (i.e., water) pressure. The pressure transducers and the solenoid valve control were the same as those used on the pre-detonator.

For steady-state flow, the atomizer flow was recorded on video, with the spray duration taken from the time annotation at the commencement and cessation of the flow. Spray duration was typically maintained around 25 seconds. After cessation, the change in water column volume was measured using a graduated cylinder. The change in volume divided by the duration of the spray was the volumetric flow rate of the liquid. Multiplying by the density yielded the mass flow rate. The mass flow rate for each oxygen pressure at each fuel pressure was plotted versus oxygen pressure. A linear curve fit was applied to the data from each fuel pressure. The results are shown in Figure 24.

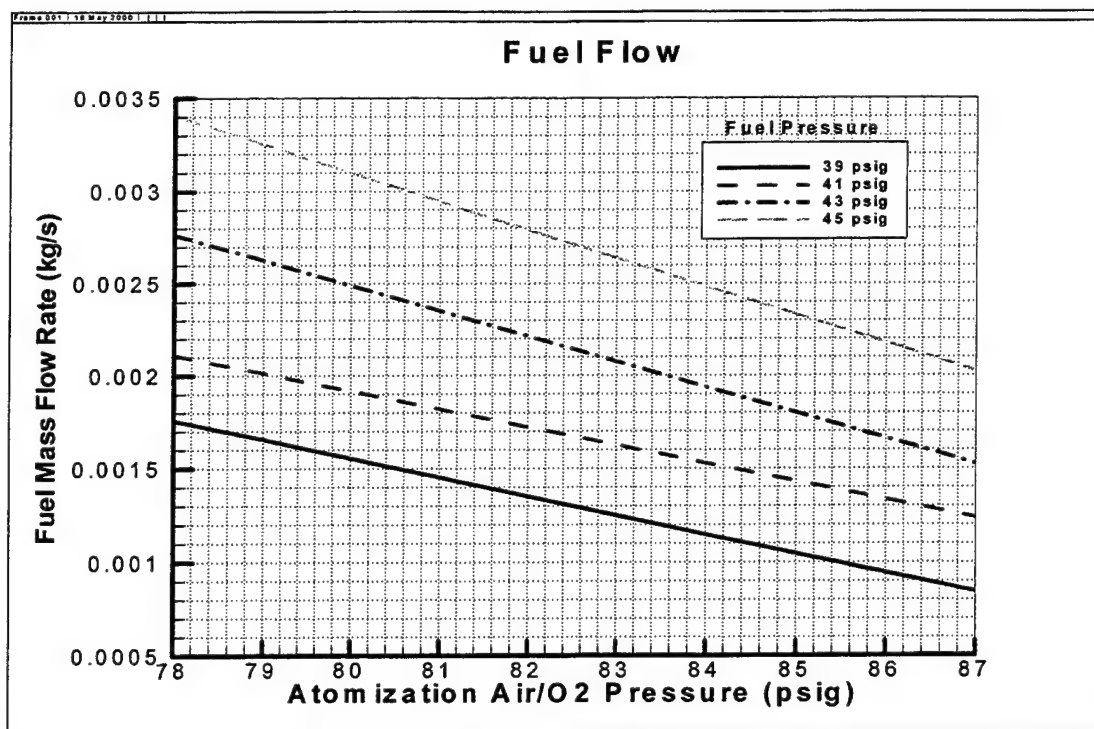


Figure 24. Atomizer Fuel Mass Flow Rate

A similar method was used to measure the mass flow rate at different duty cycles. Pulses of 500 ms, 250 ms, and 100 ms were examined using the timing in the pre-detonator control code. The atomizer was pulsed at the pressure combinations above until several seconds of total on-time had been achieved. Then the change in water level was measured and the mass flow rate calculated as above. Transient effects were found to be significant, with each shorter pulse increment increasing mass flow rate on the order of 20% compared to the last. In addition, the oxygen pressure exhibited a roughly exponential decay of approximately 3 psi over the first 100 ms of the flow. Since the pulses used for detonation are typically a factor of two to four shorter than that, a method of estimating mass flow rate from initial fuel and oxygen pressures would have to be experimentally determined for each individual pulse duration selected. Instead, it was

decided to calculate instantaneous mass flow rate every time the atomization oxygen and fuel pressures were updated in the code, using values interpolated from the linear curve fits of the steady-state data.

#### ***b. Oxygen Mass Flow Rate***

The mass flow rate of oxygen through the atomizer was calculated using an evacuated cylinder and the ideal gas law. One end of the cylinder was fastened to the nozzle of the atomizer and the other end to a pressure transducer and a vacuum pump. The volume of the cylinder and connective tubing (2648 ml) was measured using water.

After the cylinder was evacuated, the vacuum pump was isolated and steady spray was initiated until pressure in the flask reached 15 to 17 psia. Cylinder pressure was plotted versus time and two points were selected from the linear range of the plot. The change in volume of the water column was measured using a graduated cylinder, as above, and both the water and the oxygen were at ambient temperature (measured using a thermocouple). Then the ideal gas law was used to calculate oxygen mass flow rate:

$$\frac{P_2 - P_1}{t_2 - t_1} (V_{cyl+tube} - V_{water}) = \dot{m}_{O_2} \frac{\bar{R}}{M_{O_2}} T \quad (17)$$

where  $\bar{R}$  is the universal gas constant ( $8314.3 \text{ J/kgmol K}$ ) and  $M_{O_2}$  is the molecular mass of oxygen ( $31.9988 \text{ kg/kgmol}$ ).

This was repeated for several oxygen and fuel pressures over the range above. The mass flow rate for each oxygen pressure at each fuel pressure was plotted versus oxygen pressure. Over this range, oxygen mass flow rate was found to be



practically independent of fuel pressure, so a linear curve fit was applied to all the data.

The results are given in Figure 25.

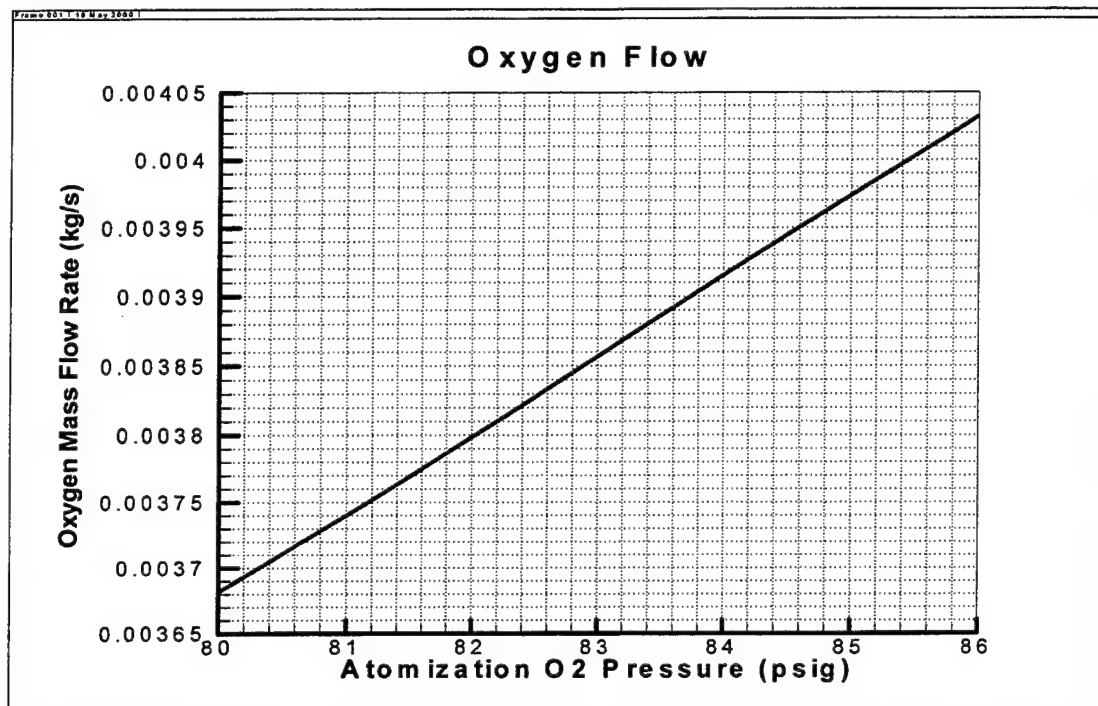


Figure 25. Atomizer Oxygen Mass Flow Rate

## B. EQUIVALENCE RATIO

### 1. Pre-Detonator

Equivalence ratio is defined as the ratio of the actual fuel-to-oxidizer mass ratio to the stoichiometric fuel-to-oxidizer mass ratio. TEP provided the stoichiometric oxidizer-to-fuel ratio for the combustion of JP-10 in oxygen (3.2882).

Instantaneous values of the equivalence ratio of the oxygen-and-atomized-fuel mixture being injected were calculated by entering the measured oxygen pressure in the linear curve fits of oxygen and fuel mass flow rates (Figures 24 and 25), interpolating fuel mass flow for the measured fuel pressure, and multiplying by the stoichiometric

oxidizer-to-fuel ratio from TEP. Equivalence ratios in the pre-detonator are illustrated in Figure 26.

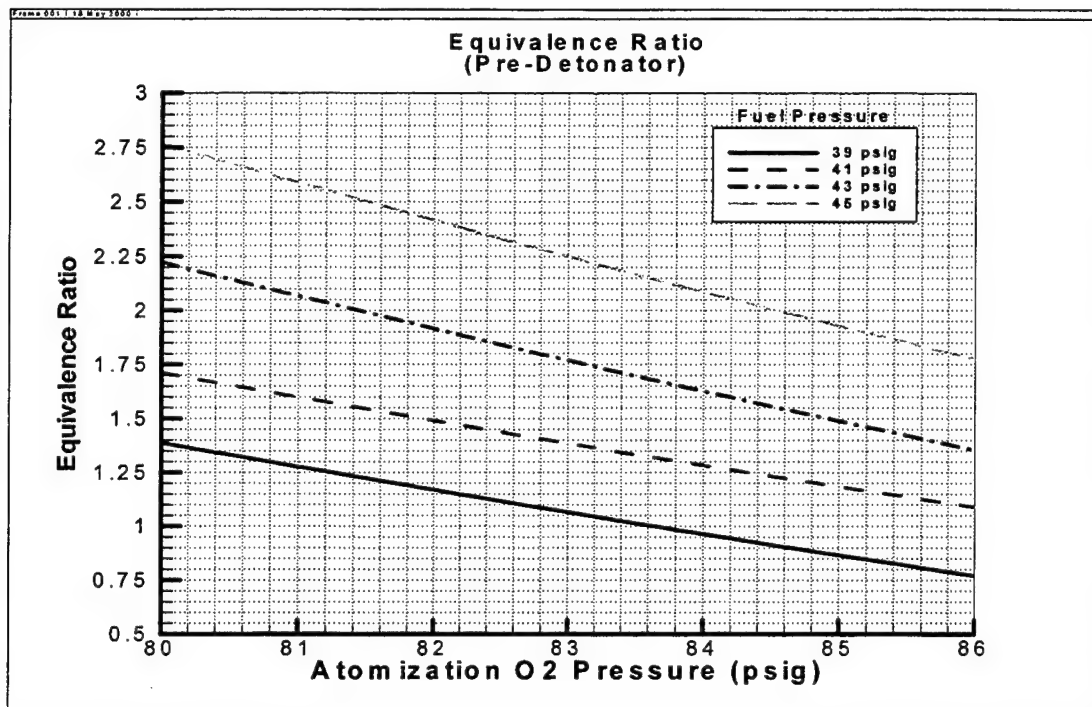


Figure 26. Pre-Detonator Equivalence Ratio

## 2. Main Combustor

The equivalence ratio in the main combustor was essentially the same as that of the air arms. Fuel mass flow rate through each atomizer was determined using the same plot as for the pre-detonator, except with atomization air pressure as the independent variable. Here, however, there are two oxidizer flows that must be considered: atomization air and main air.

The molar flow rate of air through the atomizer is assumed to be the same as that for oxygen. Thus the mass flow rate of air through the atomizer was calculated using the same data as in Section A, with only the value of the molecular mass changed

( $M_{air} = 28.966 \text{ kg/kgmol}$ ). The main air mass flow rate in each air arm was determined using volumetric flow rate curves supplied by the valve manufacturer. Multiplying the volumetric flow rate at a given inlet pressure by the density of air at standard temperature and pressure yielded the mass flow rate. This constant was added to the linear curve fit of atomization air mass flow rate to yield total air mass flow rate in each air arm versus atomizer air pressure. This was performed for main air inlet pressures of 100 psig and 150 psig. Over the pressure ranges considered here, main air flow is approximately an order of magnitude greater than atomization air flow.

Since the only significant oxidizer in air is oxygen, the stoichiometric oxidizer-to-fuel mass ratio is the same as that for the pre-detonator. However, since only 20.95% of air (by mass) is oxygen, the actual mass flow rate of air must be multiplied by this fraction. Instantaneous values of the equivalence ratio of the air-and-atomized-fuel mixture entering the air arms were calculated by entering the measured atomization air pressure in the linear curve fits of air and fuel mass flow rates, interpolating both fuel mass flow for the measured fuel pressure and air mass flow for the measured main air inlet pressure, and multiplying by the stoichiometric oxidizer-to-fuel ratio from TEP. Equivalence ratios in the main combustor are presented in Figures 27 and 28.

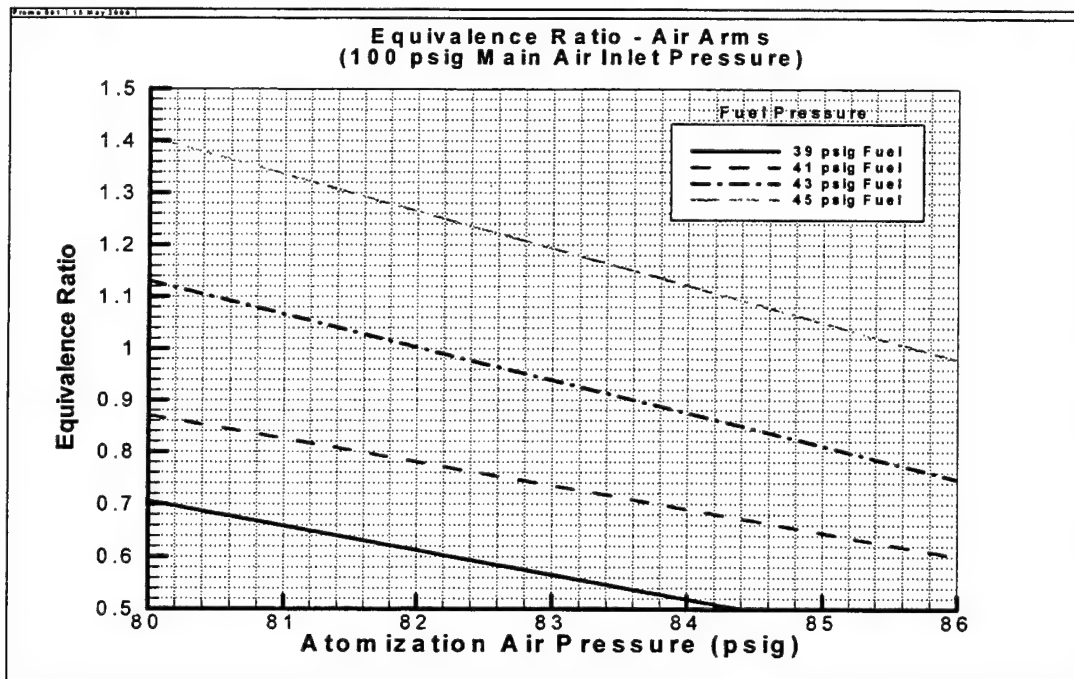


Figure 27. Main Combustor Equivalence Ratio (100 psig Main Air)

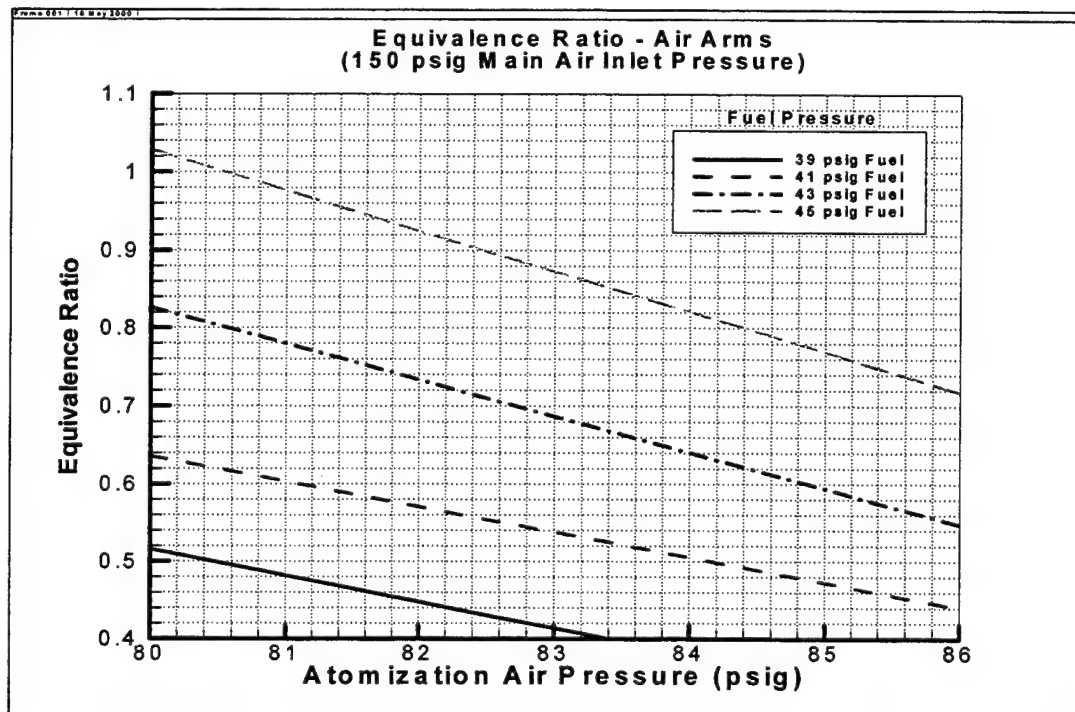


Figure 28. Main Combustor Equivalence Ratio (150 psig Main Air)

THIS PAGE INTENTIONALLY LEFT BLANK.

## VI. RESULTS

### A. TESTING

Initially, the pre-detonator was tested to determine optimum conditions. It was quickly determined that the presence of the 5-inch diameter main combustor tube had a noticeable effect on pre-detonator operation. Operating stand-alone (i.e., exhausting to atmosphere), the best pre-detonator operation occurred with a fuel fill time of 22 ms, with oxygen flow beginning 3 ms earlier. Ignition was delayed 20 ms after securing fuel/oxygen injection to allow mixing. The best operation of the pre-detonator when exhausting into the 5-inch diameter tube occurred with fuel fill times of 26-30 ms and total oxygen delivery time of 100 ms, where oxygen pressure at the atomizer was between 83.5 and 84 psig and fuel pressure was 43 psig. This condition resulted in average wave speeds of over 2300 m/s (determined using the time between pressure spikes at transducers with a known separation distance).

The pre-detonator was then tested with main air flow in the air arms. Main air was supplied to the solenoid valves at approximately 100 psig and pre-detonator oxygen and fuel pressures were maintained as above. Total oxygen delivery time and ignition delay were kept at 100 ms and 20 ms, respectively, and main air flow was secured 30 ms before ignition. Under these conditions, fuel fill times from 30-40 ms yielded average wave speeds over 2000 m/s, with detonations occurring in three or four pulses out of five. A fuel fill time of 37 ms resulted in four of five pulses detonating and each of the detonations being overdriven.

A sample timeline illustrating the various timing parameters is presented in Figure 29.

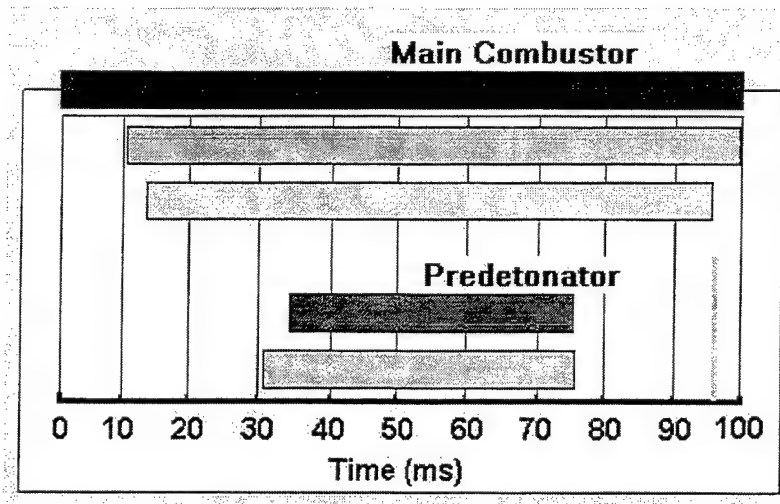


Figure 29. PDE Test Timeline

In Figure 29, zero is the start of the cycle. The first three bars (top to bottom) indicate the periods of main air flow, atomization air flow, and main fuel flow, respectively. The last two bars indicate pre-detonator fuel flow and atomization oxygen flow. To prevent the formation of large droplets when initiating fuel flow, atomization air or oxygen flow was always established a few milliseconds earlier. The vertical line in the lower right hand corner of Figure 29 shows the point of ignition.

Finally the entire system was tested with fuel in the main combustor. With the pre-detonator and main air conditions as above, fuel fill times through the air arms were varied from 98-138 ms with atomization air pressure held at 84 psig. No detonations were generated in the main combustor. The injected fuel could be seen outside the end of the main combustor, so main fuel fill time was not the issue.

It was difficult to determine the source of the problem due to the number of variables. Table 5 indicates the ranges over which the key parameters were varied.

Parameter	Range
Atomization Oxygen Pressure	80 - 90 psig
Fuel Pressure	40 - 43.5 psig
Main Air Pressure	0 - 150 psig
Atomization Air Supply Pressure	85 - 125 psig
Ignition Delay Time in Pre-Detonator	0 - 20 ms
Main Air Secured to Ignition Time	0 - 30 ms
Main Fuel Secured to Ignition Time	0 - 32 ms
Pre-Detonator Fuel Fill Time	30 - 90 ms
Main Combustor Fuel Fill Time	98 - 165 ms
Fuel Temperature	19 - 204 °C

Table 5. Testing Ranges of PDE Parameters

Although every combination of variables could not be tested, a sufficient range was tested to determine that something beyond the scope of these parameters could be causing the problem. In addition, several specific steps were taken to address possible problems. Delays between flow events and ignition were increased to try to improve fuel/oxidizer mixing. Long main combustor air purges were used to remove exhaust gases and prevent ignition of the mixture by residual combustion in the tube. Long pre-detonator oxygen and fuel/oxygen purges were used to remove exhaust gases from the pre-detonator and increase the oxygen concentration at the head end of the main



combustor. None of these were effective in enabling the formation of a detonation wave in the main combustor.

Since flowing water through the atomizer produced droplet size distributions almost the same as those of JP-10, it was assumed that the volumetric flow rate would be the same as well. However, subsequent testing has demonstrated that even with the same droplet size distribution, the volumetric flow rate for JP-10 is approximately 20% higher than that for water. Thus all tests were conducted at a higher equivalence ratio than predicted. However, since equivalence ratio was varied over such a wide range, this did not substantially affect the overall results.

The vapor pressure of the fuel was increased by heating the fuel up to 204°C. From Reference 14, JP-10 vapor pressure increases from 0.31 kPa at 20°C to 21.0 kPa at 120°C. Extrapolating this out to 204°C yields a value of approximately 175 kPa. Unfortunately, even this could not generate a detonation in the main combustor. However, the increased fuel mass flow rates at these elevated temperatures were not accurately determined, so although the equivalence ratio was varied over a considerable range so as to examine both lean and rich mixtures, the actual values were not known.

The installation of a 0.625-inch thick cylindrical quartz section allowed the presence of fuel in the head end of the main combustor to be confirmed optically via laser transmission. Testing was conducted to determine the pre-detonator fuel fill time (at different fuel and atomizer oxygen pressures) required for fuel to reach the main combustor. Over our pressure ranges, the longest fuel fill time required was 57 ms.

Finally, the Princeton Instruments CCD camera was used to attempt to determine what was happening when the detonation wave exited the pre-detonator. The gate width was set at  $0.5\ \mu\text{s}$  and the gating itself was triggered (with a delay) from a pressure transducer in the pre-detonator. Figure 30 illustrates a typical detonation failure (i.e., a simple deflagration).

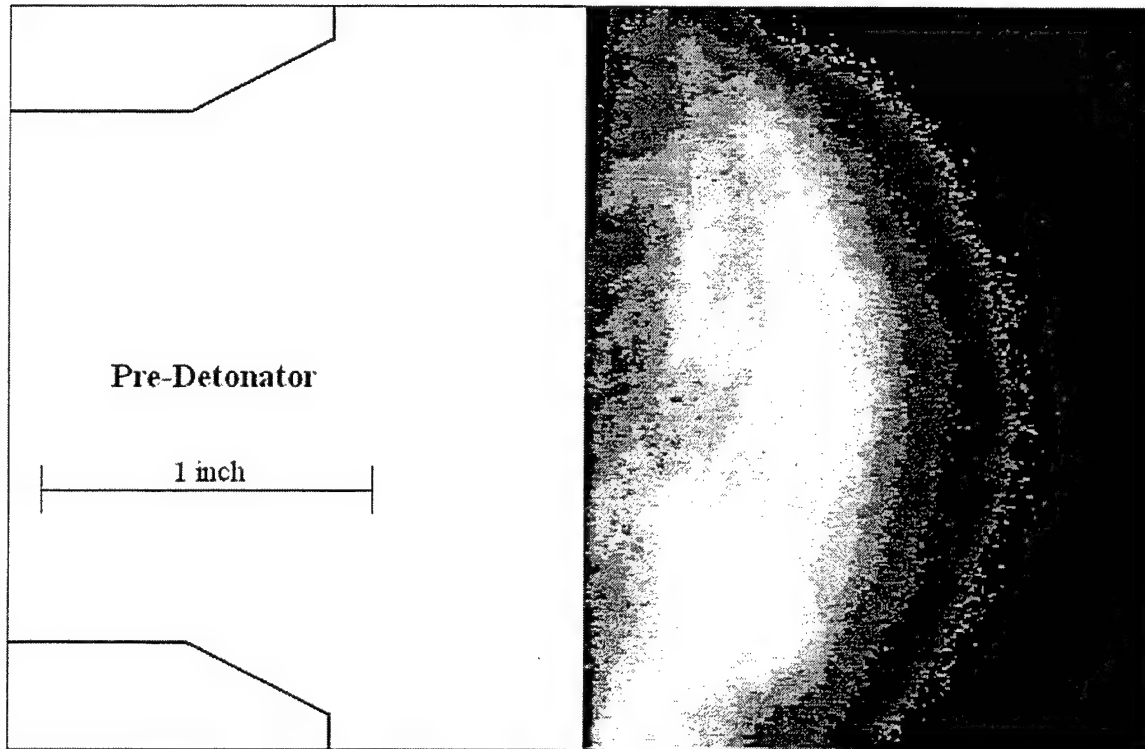


Figure 30. Failed Detonation

For comparison, Figure 31 illustrates a detonation from the pre-detonator propagating into the main combustor.

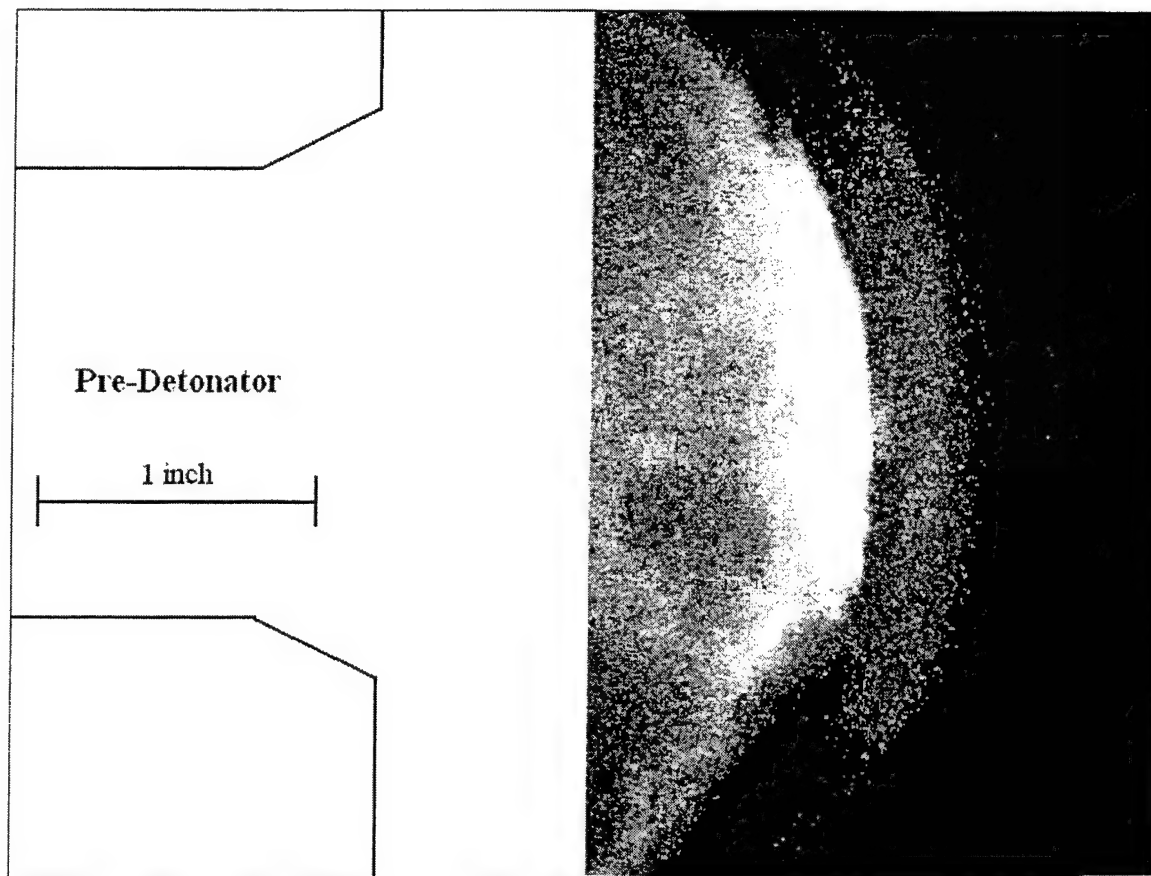


Figure 31. Detonation Propagating from Pre-Detonator into Main Combustor

The core detonation is clearly visible, as is the detonation failure around the perimeter due to the rarefaction waves propagating radially inward. This shows that the detonation front did not transition from planar to spherical. Without re-initiation of detonation at the tube wall, the detonation will fail.

In an attempt to image a successful detonation transmission into the main combustor, ethylene and oxygen were used. Although detonation was successfully re-initiated, the event shattered the quartz, as shown in Figure 32.

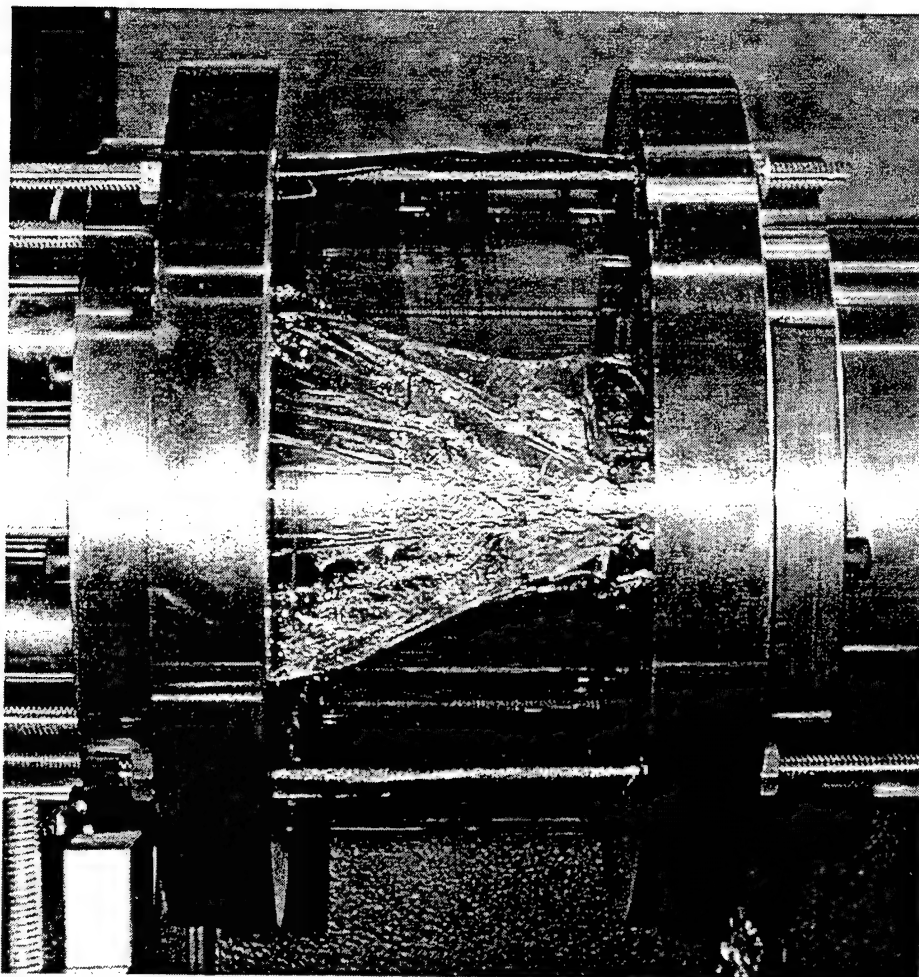


Figure 32. Shattered Quartz Section

Extremely high pressures can be observed at re-initiation, occasionally exceeding 3000 psi.

#### **B. FAILURE THEORIES**

Several factors complicate analysis of the detonation propagation in this study. Diffraction into an unconfined volume and propagation into a mixture of different detonability are complex events individually but having both occur simultaneously greatly increases the complexity. Furthermore, aerosol detonations have not been thoroughly studied and the effects of droplet size distribution, mixing, evaporation, and

two-phase combustion add another level of complexity over gaseous detonations. Lastly, detailed chemical kinetics for JP-10 are just now being studied and have not yet been analyzed to a level which could aid in PDE design.

The resulting uncertainties are crucial. Since it is generally accepted that all detonation parameters with dimensions of length are governed by cell size, the fact that JP-10 cell size as a function of nitrogen dilution and equivalence ratio is not known becomes very significant. If the cell size of a JP-10/air aerosol detonation at an equivalence ratio of 1.0 were much larger than assumed, the main combustor could be smaller than the limiting tube diameter. Below this critical limit, even a single-headed spinning detonation would not form [Ref. 9]. It seems highly unlikely that JP-10 cell size would be so much larger than that of JP-4, but the example of methane demonstrates that there can be extreme differences between hydrocarbon fuels.

Figure 30 shows a detonation wave leaving the pre-detonator that does not transition from planar to spherical when it enters the main combustor. There are several possible causes for this including non-uniform fuel distribution at the head end of the main combustor, a mixture outside detonability limits, an excessive fraction of the fuel in droplets too large to support detonation, JP-10/oxygen cell size greater than 3.05 mm, or the empirical law (Equation 7) simply may not hold in this case.

Another potential problem is the particular geometry at the end of the pre-detonator. As indicated in the Appendix, the diameter of the pre-detonator actually increases near the exit, from 1.5625 inches to 2.0 inches. This increases the effective diameter at the point the detonation enters the main combustor, thereby improving the

potential for transition to a spherical wave front or, alternately, allowing greater time to re-initiate detonation at the boundary before the core detonation is quenched. However, this minor initial diffraction occurs only 0.4375 inches (11.1125 mm) from the plane of the main combustor. Murray and Lee [Ref. 11] report that a detonation requires approximately 12 cell widths of travel to recover from a boundary-induced disturbance. That implies that if the JP-10/oxygen cell size in the pre-detonator exceeds 0.926 mm, the initial diffraction actually weakens the detonation entering the main combustor.

Since the detonation is occurring in a two-phase mixture, the liquid droplets (especially the larger ones) almost certainly burn later than the vaporized portion of the fuel. This would create a complex and irregular cellular structure. Edwards and Thomas (as discussed in Reference 10) suggest that detonations with such structure could require a diameter of more than 10-13 cell widths for successful transmission across an abrupt expansion. Benedick, et al [Ref. 17], contend that relatively insensitive fuels, such as hydrocarbon propulsion fuels, cannot even achieve detonation unless the fuel has vaporized. Figure 33 shows the approximate distance behind the detonation front at which fuel droplets of varying size vaporize.

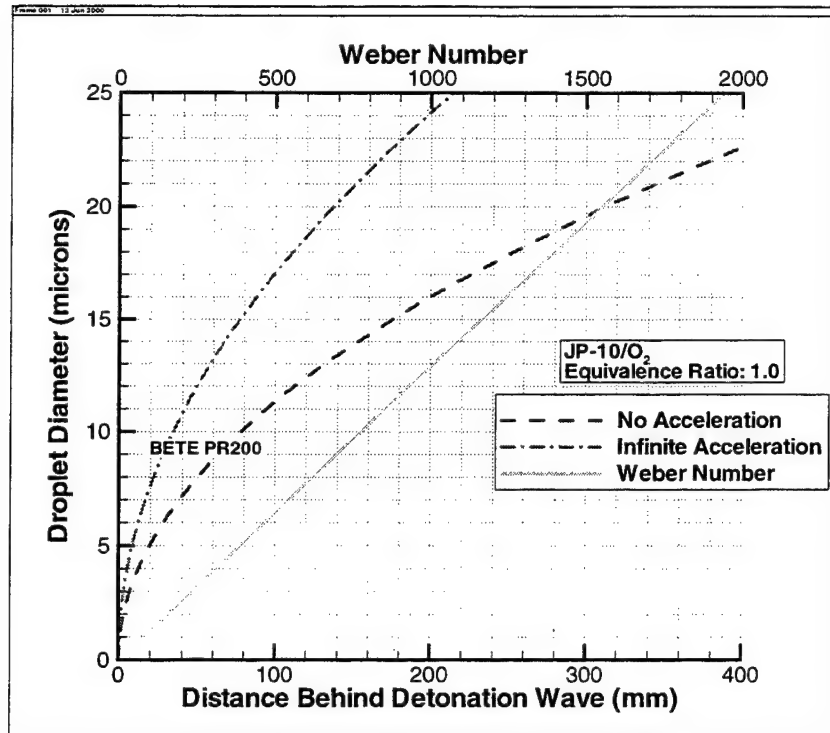


Figure 33. Fuel Vaporization Behind the Detonation front From Ref. [21]

For the fuel droplet distributions achieved here, (SMDs of less than 10 microns) the results would be close to the infinite acceleration curve. Since the distance behind a detonation at which chemical energy release can contribute to the wave is generally taken to be approximately 1 cm, a considerable fraction of the fuel is either detonated before complete vaporization or simply burns well behind the wave.

Since the JP-10/oxygen detonation is much more energetic than JP-10/air, detonations in the pre-detonator would become overdriven detonation waves in the JP-10/air. The more highly overdriven the detonation, the smaller the cell size and the more regular the structure [Ref. 10]. This is an important premise upon which this whole testing program was based. Table 6 gives an indication of the degree to which the detonation entering the JP-10/air aerosol was overdriven.

	JP-10 / Air	JP-10 / Oxygen		
Equivalence Ratio	1.0	1.0	1.5	2.0
Pressure Ratio	18.464	39.096	48.589	54.151
Detonation Velocity ( $m/s$ )	1786.6	2299.7	2475.5	2543.0
$DetV_{O_2}/DetV_{Air}$	1	1.287	1.386	1.423

Table 6. Detonation Parameters by Mixture

Table 6 uses C-J detonation values from TEP. The last row in the table shows detonation velocity normalized by C-J detonation velocity in the main combustor (i.e., JP-10/air aerosol). Since the pre-detonator was typically operated at an equivalence ratio between 1.5 and 2.0, the detonation entering the main combustor was significantly overdriven. Unfortunately, this was insufficient to generate a spherical detonation front in the JP-10/air aerosol.

The other mechanism for direct initiation of a detonation in the main combustor is through the creation of reignition nuclei at the boundary. Several factors were present that eliminated this possibility. First and foremost, the ratio of main combustor diameter to pre-detonator diameter (see the Appendix) made this unlikely, if not impossible. The distance from the pre-detonator to the wall of the main combustor is only slightly less than the diameter of the pre-detonator, a ratio of approximately 0.8. For both JP-10/oxygen and JP-10/air, the detonation wave propagates at just over 1.8 times sonic velocity in the burned gases, thereby travelling 0.9 pre-detonator diameters before being quenched. Thus the oblique shock barely reaches the tube wall before the core detonation is quenched, leaving almost no time for the formation of reignition nuclei.



The only reason the oblique shock has time to reach the wall at all is because the pre-detonator tube diameter was expanded from 1.5625 inches to 2.0 inches near the end. However, as discussed above, this diffraction occurs too close to the end of the tube to allow the detonation to fully recover from the disturbance, so the detonation entering the main combustor is somewhat weakened. Furthermore, due to purging of the pre-detonator before each cycle, the oxygen concentration in the main combustor is probably slightly higher on the axis than at the wall. This would increase sonic velocity in the burned gases and thereby accelerate the rarefaction waves quenching the core detonation, thus allowing even less time to re-initiate detonation at the boundary.

Compounding the geometry problems hindering reignition is the initiation delay (noted by Desbordes and Lannoy [Ref. 12]) before detonation transmission into the less sensitive air mixture. Together these factors would seem to ensure that the core detonation would be quenched well before reignition nuclei could be formed at the wall. Even without the geometry concerns, there remains the question of whether a detonation can be re-initiated at all if the chemical reaction time doubles going from one mixture to another.

## **VII. CONCLUSIONS**

### **A. SUMMARY**

Several complex conditions existed for this testing. A two-phase mixture is by definition non-homogeneous, thereby making detonation dependant upon droplet size, mixing and vaporization. Moreover, this would tend to produce a multi-modal detonation structure, consisting of large and irregular cells. Propagation of such a detonation across a geometric diffraction with simultaneous composition change is an extremely complicated process.

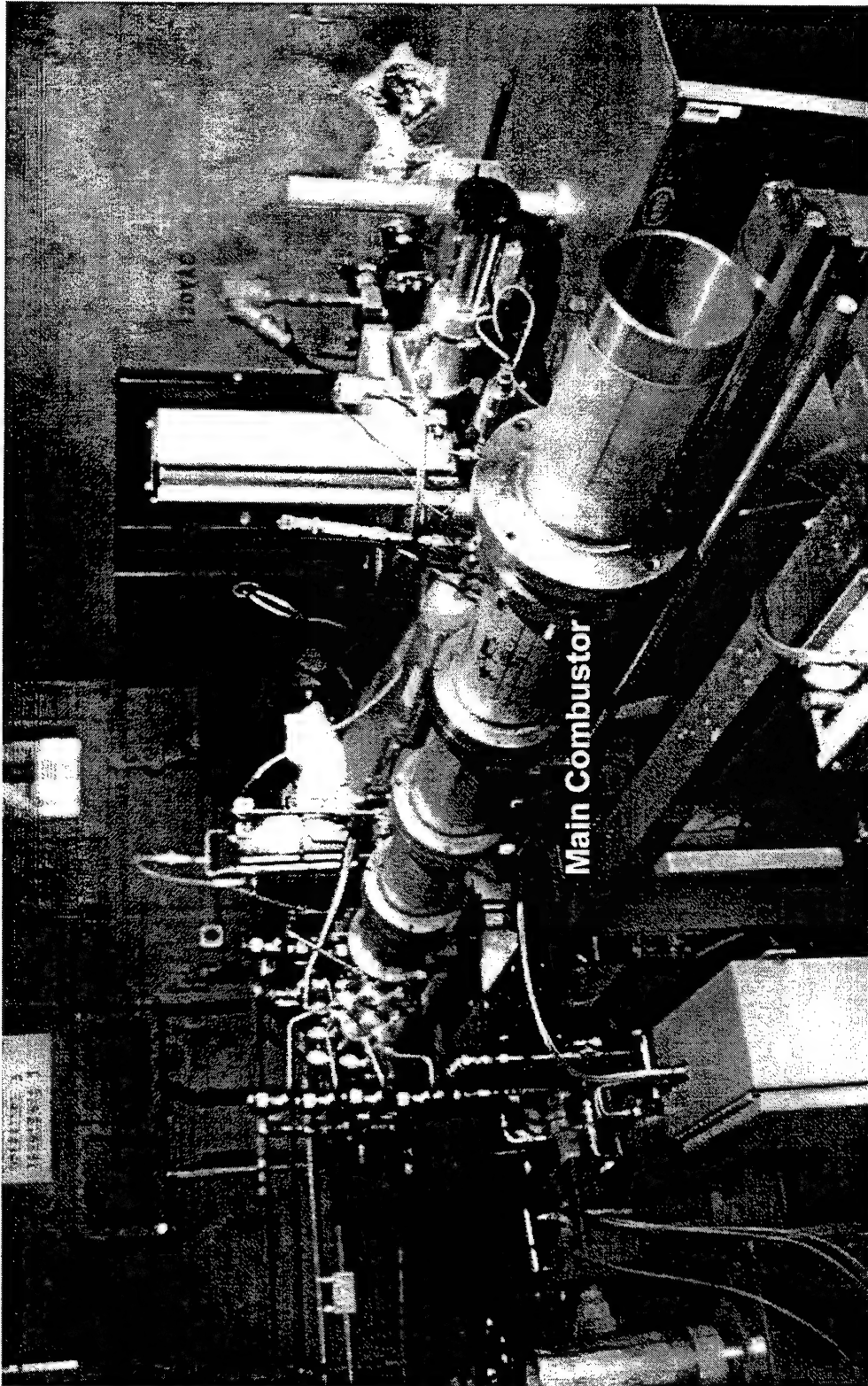
Under the conditions tested here, the pre-detonator was shown to be insufficient (in energy, diameter, or both) to allow transition from a confined planar detonation to an unconfined spherical detonation. At the same time, the main combustor diameter was too large to allow re-initiation of detonation at the tube wall. The change in chemical kinetics between the mixtures (as well as likely fuel and oxygen non-uniformity) further hindered the transmission process.

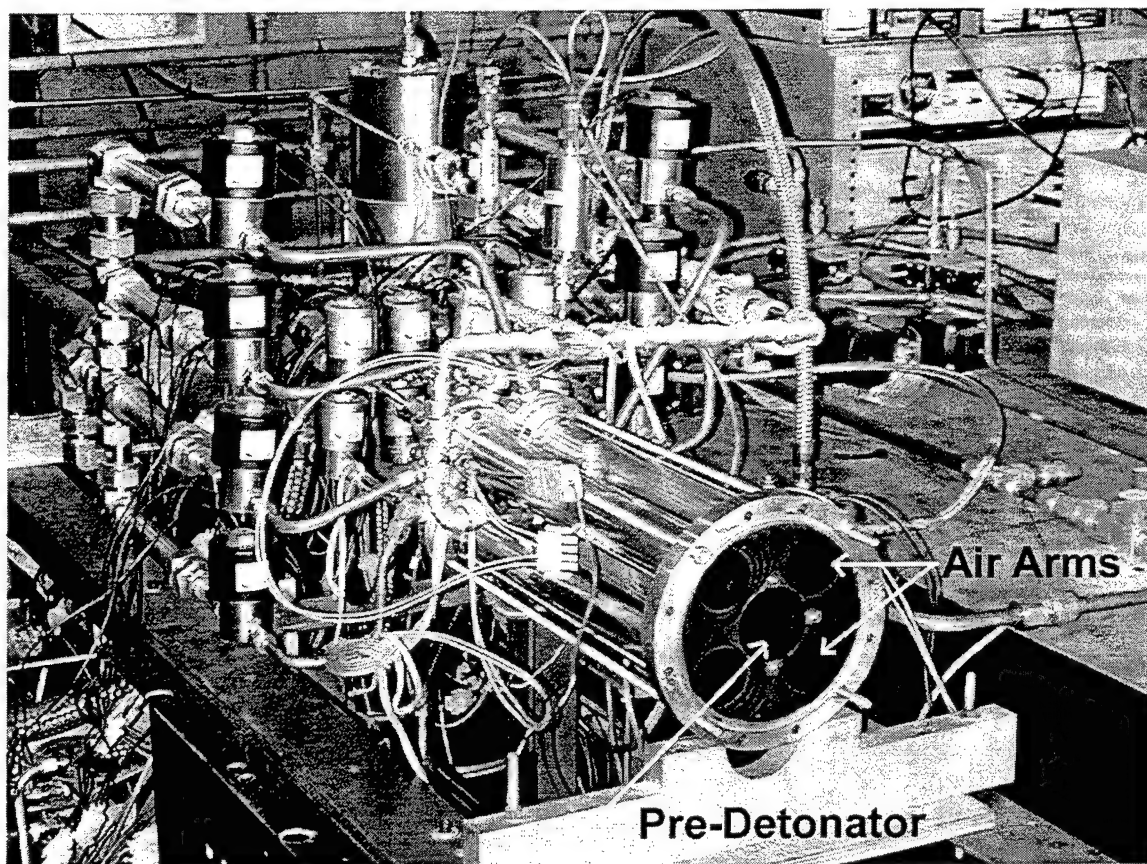
### **B. RECOMMENDATIONS**

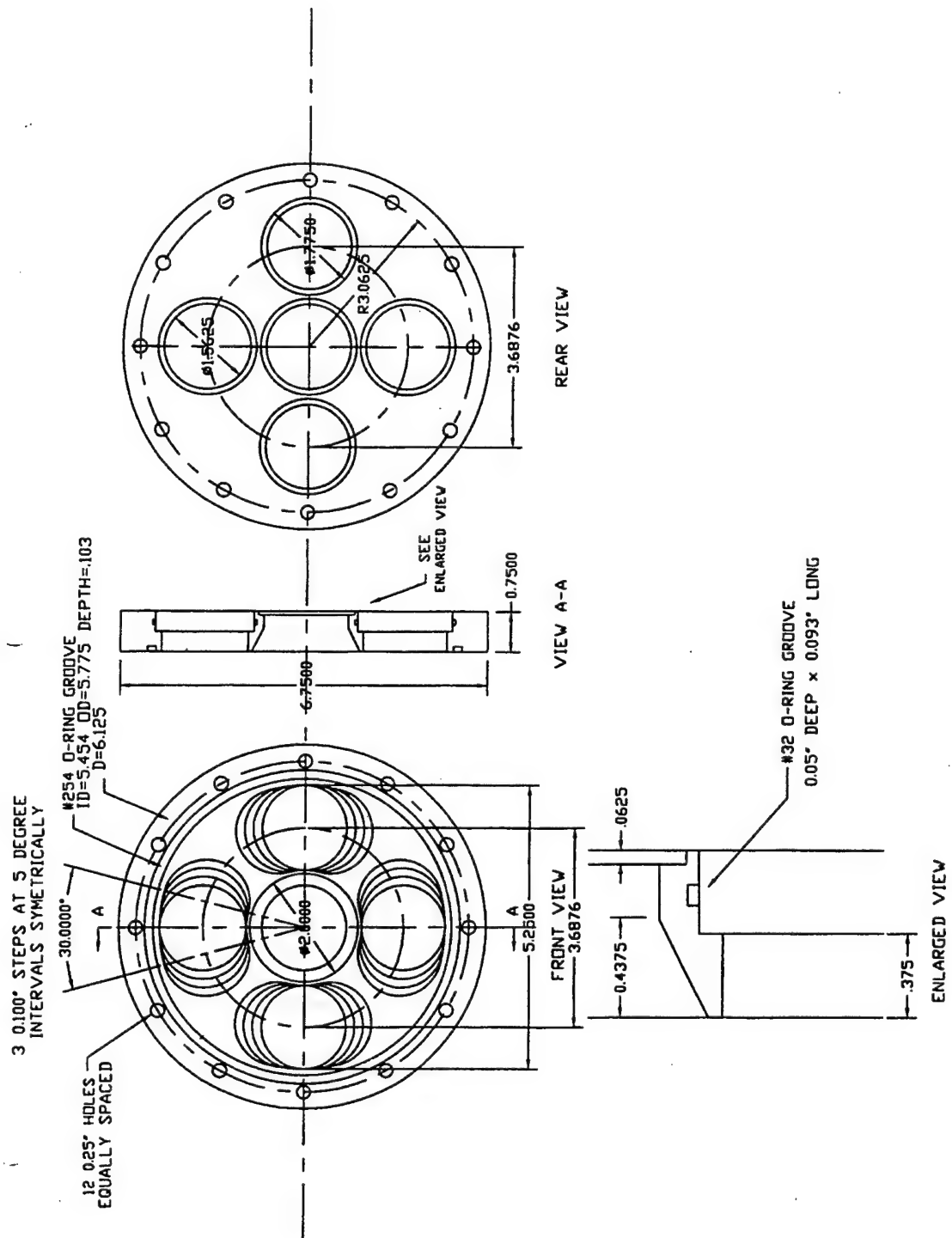
Tests should be performed to clarify conditions at the head end of the main combustor. First of all, the distributions of both fuel and oxygen at the end of the pre-detonator and in the head end of the main combustor should be mapped axially and radially. Since JP-10/oxygen detonations are highly repeatable while JP-10/air detonations have been as of yet unattainable, detonability of JP-10 as a function of oxygen concentration could be tested. Also, an evitiator can be used to vary the degree of vaporization of the fuel before detonation. Beginning with fully vaporized JP-10, fuel

droplet size should be gradually increased until the maximum Sauter mean diameter that will support detonation in a JP-10/air mixture is determined. Since the shape of the droplet distribution remains essentially unchanged, a larger SMD directly corresponds to a smaller fraction of fuel vaporized. Finally, the ratio of main combustor diameter to pre-detonator diameter should be reduced, to allow detonation re-initiation at the wall of the main combustor. Once detailed chemical kinetics and cell size information becomes available, the relative sizes of the pre-detonator and the main combustor can be optimized to minimize oxygen requirements. Alternatively, the method of Desbordes and Lannoy [Ref. 12] could be attempted, wherein the detonation propagates into the less detonable mixture before undergoing diffraction into an unconfined volume.

## APPENDIX HARDWARE







THIS PAGE INTENTIONALLY LEFT BLANK.

## LIST OF REFERENCES

1. Bauer, P., Dabora, E., Manson, N., "Chronology of Early Research on Detonation Wave," *Dynamics of Detonations and Explosions: Detonations*, Progress in Astronautics and Aeronautics Volume 133, American Institute of Aeronautics and Astronautics (AIAA), Inc., 1989.
2. Manson, N., Dabora, E., "Chronology of Research on Detonation Waves: 1920-1950," *Dynamic Aspects of Detonations*, Progress in Astronautics and Aeronautics Volume 153, AIAA, 1993.
3. Bussing, T., Pappas, G., "Pulse Detonation Engine Theory and Concepts," *Developments in High-Speed-Vehicle Propulsion Systems*, Progress in Astronautics and Aeronautics Volume 165, AIAA, 1996.
4. Zitoun, R., Daniau, E., Desbordes, D., "Specific Impulse of Reactive Mixture in Detonation Regime: Effect of the Initial Pressure," 17<sup>th</sup> International Colloquium on the Dynamics of Explosions and Reactive Systems, Heidelberg, Germany, July 25-30, 1999.
5. Glassman, I., *Combustion*, Academic Press, Inc., 1987.
6. Forster, D., "Evaluation of a Liquid-Fueled Pulse Detonation Engine Combustor," Master's Thesis, Naval Postgraduate School, Monterey, California, December, 1998.
7. Kuo, K. K., *Principles of Combustion*, John Wiley & Sons, Inc., 1986.
8. Mitrofanov, V., "Modern View of Gas Detonation Mechanisms," *Advances in Combustion Science: In Honor of Ya. B. Zel'dovich*, Progress in Astronautics and Aeronautics Volume 173, AIAA, Inc., 1997.
9. Knystautas, R., Guirao, C., Leé, J. H., and Sulmistras, A., "Measurements of Cell Size in Hydrocarbon-Air Mixtures and Predictions of Critical Tube Diameter, Critical Initiation Energy, and Detonability Limits," *Dynamics of Shock Waves, Explosions, and Detonations*, Progress in Astronautics and Aeronautics Volume 94, American Institute of Aeronautics and Astronautics (AIAA), Inc., 1984.
10. Moen, I., Funk, J., Ward, S., Rude, G., "Detonation Length Scales for Fuel-Air Explosives," *Dynamics of Shock Waves, Explosions, and Detonations*, Progress in Astronautics and Aeronautics Volume 94, American Institute of Aeronautics and Astronautics (AIAA), Inc., 1984.
11. Murray, S., Lee, J., "The Influence of Yielding Confinement on Large-Scale Ethylene-Air Detonations," *Dynamics of Shock Waves, Explosions, and Detonations*,



Progress in Astronautics and Aeronautics Volume 94, American Institute of Aeronautics and Astronautics (AIAA), Inc., 1984.

12. Desbordes, D., Lannoy, A., "Effects of a Negative Step of Fuel Concentration on Critical Diameter of Diffraction of a Detonation," *Dynamics of Detonations and Explosions: Detonations*, Progress in Astronautics and Aeronautics Volume 133, American Institute of Aeronautics and Astronautics (AIAA), Inc., 1989.
13. Borisov, A., Khomik, S., Mikhalkin, V., Saneev, E., "Critical Energy of Direct Detonation Initiation in Gaseous Mixtures," *Dynamics of Detonations and Explosions: Detonations*, Progress in Astronautics and Aeronautics Volume 133, American Institute of Aeronautics and Astronautics (AIAA), Inc., 1989.
14. Thermo-Chemical Equilibrium Program (TEP), Software and Engineering Associates, Inc., Carson City, Nevada.
15. *Handbook of Aviation Fuel Properties*, Coordinating Research Council, 1988.
16. Beeson, H., McClenagan, R., Bishop, C., Benz, F., Pitz, W., Westbrook, C., Lee, J., "Detonability of Hydrocarbon Fuels in Air," *Dynamics of Detonations and Explosions: Detonations*, Progress in Astronautics and Aeronautics Volume 133, American Institute of Aeronautics and Astronautics (AIAA), Inc., 1989.
17. Benedick, W., Tieszen, S., Knystautas, R., Lee, J., "Detonation of Unconfined Large-Scale Fuel Spray-Air Clouds," *Dynamics of Detonations and Explosions: Detonations*, Progress in Astronautics and Aeronautics Volume 133, American Institute of Aeronautics and Astronautics (AIAA), Inc., 1989.
18. "Most Frequently Asked Questions about XA Series Nozzles!" BETE Fog Nozzle Inc., Greenfield, Massachusetts.
19. Brophy, C., Netzer, D., Forster, D. "Detonation Studies of JP-10 with Air and Oxygen for Pulse Detonation Engine Development", Paper No. AIAA 98-4003, July 1998.
20. Tulis, A., and Selman, J., "Unconfined Aluminum Particle Two-Phase Detonation in Air," *Dynamics of Shock Waves, Explosions, and Detonations*, Progress in Astronautics and Aeronautics Volume 94, American Institute of Aeronautics and Astronautics (AIAA), Inc., 1984.
21. Brophy, C., Netzer, D., "Operation, Performance, and Characteristics of a JP-10/O<sub>2</sub> Fueled Pulse Detonation Engine," XIV ISABE Symposium, Florence, Italy, September 5-10, 1999.

## INITIAL DISTRIBUTION LIST

1. Defense Technical Information Center ..... 2  
 8725 John J. Kingman Road, Suite 0944  
 Ft. Belvoir, VA 22060-6218
  
2. Dudley Knox Library..... 2  
 Naval Postgraduate School  
 411 Dyer Road  
 Monterey, CA 93943-5101
  
3. Dr. David W. Netzer, Code AA/Nt ..... 2  
 Department of Aeronautics and Astronautics  
 Naval Postgraduate School  
 699 Dyer Road, Room 127  
 Monterey, CA 93943-5106
  
4. Dr. Christopher M. Brophy, Code AA/Br ..... 3  
 Department of Aeronautics and Astronautics  
 Naval Postgraduate School  
 699 Dyer Road, Room 127  
 Monterey, CA 93943-5106
  
5. Dr. Raymond P. Shreeve ..... 1  
 Department of Aeronautics and Astronautics  
 Naval Postgraduate School  
 699 Dyer Road, Room 127  
 Monterey, CA 93943-5106
  
6. LT Todd A. Hofstedt ..... 2  
 1811 102<sup>nd</sup> Circle NW  
 Coon Rapids, MN 55433
  
7. Dr. Gabriel Roy ..... 1  
 Office of Naval Research  
 Mechanics Division, Office 333  
 Ballston Tower One  
 800 N. Quincy Street  
 Arlington, VA 22217-5660

THIS PAGE INTENTIONALLY LEFT BLANK.